Dear Biogeosciences editor,

We are grateful for the involvement and suggestions of both the referees and editor, which have so far greatly improved the quality of our manuscript. The new textual suggestions of referee #1 have now also been implemented, as detailed below (responses to reviewers in bold). We hope that these adjustments in the manuscript allow publication in *Biogeosciences*.

Yours sincerely,

The authors

REVIEWER #1 COMMENTS

Remove consistently "deuterium" from the manuscript.

➔ **The word 'deuterium' is removed consistently from both the manuscripts and the supplementary data.**

L29/60. Add "relative" before "root water uptake profiles"

➔ **The word 'relative' has now been added following the reviewer suggestion. [L29, 61, 869]**

L395. You are almost there . It should read something like "and where soil water is more depleted in [2H] in comparison with the soil layers above" (i.e., not δ2H)

➔ **This sentence has been altered and now reeds as: 'Early in the morning, when transpiration is low, most of the RWU occurs in deeper layers, where soil matric potential is less negative and where soil water is more depleted in ^2H compared with the soil layers above (Fig. S8a-b).' [L394:396]**

L398/403/536-537. A δ value cannot be enriched.

➔ **These sentences have now been altered, highlighting that not the δ-value, but the sampled water is enriched. [L398, 403, 534:537, 567:568]**

L456. "to access more shallow and enriched soil layer[water]"

➔ **This sentence now reads as "Higher SF_t requires more negative $\widehat{\Psi}_{X,0,t}$, enabling the plant to access the enriched soil water of more shallow soil layers". [L455:456]**

L478-479. Correct terminology "…isotope…"

➔ **The terminology is now corrected and the sentence reads as follows: 'However, as diffusion is proportional to the time that water isotopologues remain in the xylem, its absolute impact on δ^2H_X is negligible in plants with a high true sap flow velocity'. [L466:468]**

Causes and consequences of pronounced variation in the isotope composition of plant xylem water

Hannes P.T. De Deurwaerder [(1,2)*], Marco D. Visser [(2)], Matteo Detto [(2)], Pascal Boeckx [(3)], Félicien Meunier [(1,4)], Kathrin Kuehnhammer [(5,6)], Ruth-Kristina Magh [(7,8)], John D. Marshall [(8)], Lixin Wang [(9)], Liangju Zhao [(10,11)], Hans Verbeeck [(1)]

(1) CAVElab - Computational & Applied Vegetation Ecology, Faculty of Bioscience Engineering, Ghent University, Ghent, Belgium
(2) Department of Ecology and Evolutionary Biology, Princeton University, Princeton, NJ, USA
(3) ISOFYS – Isotope Bioscience Laboratory, Faculty of Bioscience Engineering, Ghent University, Ghent, Belgium
(4) Ecological Forecasting Lab, Department of Earth and Environment, Boston University, Boston, Massachusetts, USA
(5) IGOE, Umweltgeochemie, Technische Universität Braunschweig, Braunschweig, Germany
(6) Ecosystem Physiology, University of Freiburg, Freiburg, Germany,
(7) Institute for Forest Sciences, Chair of Tree Physiology, University of Freiburg, Freiburg, Germany
(8) Department of Forest Ecology and Management, SLU, Swedish University of Agricultural Sciences, Umeå, Sweden
(9) Department of Earth Sciences, Indiana University-Purdue University Indianapolis (IUPUI), Indianapolis, IN 46202, USA
(10) Shaanxi Key Laboratory of Earth Surface System and Environmental Carrying Capacity, College of Urban and Environmental Sciences, Northwest University, Xi'an 710127, China
(11) Key Laboratory of Ecohydrology and Integrated River Basin Science, Northwest Institute of Eco-Environment and Resources, Chinese Academy of Sciences, Lanzhou 730000, China

**Correspondence to*: Hannes De Deurwaerder (Hannes_de_deurwaerder@hotmail.com)

Abstract

1. Stable isotopologues of water are widely used to derive relative root water uptake (RWU) profiles and average RWU depth in lignified plants. Uniform isotope composition of plant xylem water (δ_{xyl}) along the stem length of woody plants is a central assumption of the isotope tracing approach, which has never been properly evaluated.

2. Here we evaluate whether strong variation in δ_{xyl} within woody plants exists using empirical field observations from French Guiana, northwestern China, and Germany. In addition, supported by a mechanistic plant hydraulic model, we test hypotheses on how variation in δ_{xyl} can develop through the effects of diurnal variation in RWU, sap flux density, diffusion, and various other soil and plant parameters on the δ_{xyl} of woody plants.

3. The hydrogen and oxygen isotope composition of plant xylem water shows strong temporal (i.e., sub-daily) and spatial (i.e., along the stem) variation ranging up to 25.2‰ and 6.8‰ for δ^2H and $\delta^{18}O$ respectively, greatly exceeding measurement error range in all evaluated datasets. Model explorations predict that significant δ_{xyl} variation could arise from diurnal RWU fluctuations and vertical soil water heterogeneity. Moreover, significant differences in δ_{xyl} emerge between individuals that differ only in sap flux densities, or are monitored at different times or heights.

4. This work shows a complex pattern of δ_{xyl} transport in the soil-root-xylem system, which can be related to the dynamics of RWU by plants. These dynamics complicate the assessment of RWU when using stable water isotopologues, but also open new opportunities to study drought responses to environmental drivers. We propose to include monitoring of sap flow and soil matric potential for more robust estimates of

52 average RWU depth and expansion of attainable insights in plant drought strategies and
53 responses.
54

55 **Keywords**
56 Ecohydrology, Lianas, Root water uptake, Sap flow, Stable isotope composition of water,
57 Tropical trees, Water competition

58

1. Introduction

The use of stable isotope composition of water has strengthened ecohydrology studies by providing insights into phenomena that are otherwise challenging to observe, such as relative root water uptake depth (RWU depth) (Rothfuss & Javaux, 2017), below-ground water competition and hydraulic lift (Hervé-Fernández *et al.*, 2016; Meunier *et al.*, 2017). Compared to root excavation, the technique is far less destructive and labor-intensive. This makes it more flexible for studying multiple individuals across spatial and temporal scales (i.e. individual to ecosystem, daily to seasonal) (Dawson *et al.* 2002). Besides, the study of stable isotope composition of xylem water measures the real effects of RWU at different depths whereas excavation yields only root distribution and architecture. The advantages and wide applicability of this method make it a popular technique that pushes the boundaries of ecohydrology (Dawson *et al.*, 2002; Yang *et al.*, 2010; Rothfuss & Javaux, 2017; Lanning *et al.*, 2020)

A variety of methods are used to infer average RWU depth from the isotope composition of plant xylem water (δ_{xyl}), but all rely on a direct relationship between the isotopic compositions of plant xylem and soil water (Ehleringer & Dawson, 1992). All have two key assumptions. The first is that the isotope composition of plant xylem water remains unchanged during transport from root uptake to evaporative sites (e.g. leaves and non-lignified green branches). Hence, isotopic fractionation – i.e. processes that cause a shift in the relative abundances of the water isotopologues, driven by their differences in molecular mass – do not occur during the transport from the uptake to the evaporative site (Wershaw *et al.*, 1966; Zimmermann *et al.*, 1967; White *et al.*, 1985; Dawson & Ehleringer, 1991; Walker & Richardson, 1991; Dawson *et al.*, 2002; Zhao *et al.*, 2016). Second, all methods assume that xylem water provides a well-mixed isotope composition of water from different soil layers: sampled xylem water instantaneously reflects the distribution and water uptake of the roots independent of the timing or height of sampling.

The first assumption is relatively well supported. Isotopic fractionation at root level does not raise concerns for most RWU assessments using water isotopologues (Rothfuss & Javaux, 2017) except for kinetic fractionation that might occur during water transported across the root membrane in extreme environments (Lin & Sternberg, 1993; Ellsworth and Williams, 2007; Zhao *et al.*, 2016). Similarly, isotopic fractionation of water within an individual plant, although possible, is generally not considered a serious problem (Yakir, 1992; Dawson & Ehleringer, 1993; Cernusak *et al.*, 2005; Mamonov *et al.*, 2007; Zhao *et al.*, 2016). This perception was recently contested by Barbeta *et al* (2020), advocating a more general nature of the occurrence of isotopic offsets between xylem water and potential water sources. As the origin of these offsets remains debated, future research should clarify its impact on the applicability of stable water isotopic compositions for RWU assessment. However, the second assumption of time and space invariance of the isotope composition of xylem water has, to our knowledge, never been assessed.

Various plant physiological processes, ranging from very simple to more complex mechanisms, could influence within plant variation in δ_{xyl} at short time scales, i.e. sub-daily to sub-hourly. For instance, plant transpiration during the day is regulated by stomata according to water supply and atmospheric demand, and follows well known diurnal patterns (Steppe & Lemeur, 2004; Epila *et al.*, 2017). This results in a changing water potential gradient between soil and leaves throughout the day (Fig 1a,b), which in turn affects the depth of the average RWU (Goldstein *et al.*, 1998; Doussan *et al.*, 2006; Huang *et al.*, 2017). Hence, shifts in a plant's capacity to take up water at different soil layers during the day can generate diurnal variation in the mixture of isotope composition from water taken up from various depths (Fig 1c). Subsequently, this water mixture moves up along the xylem with the velocity of the sap flux density. As these sap flux densities depend on species and individual-specific hydraulic traits and their responses to atmospheric water demand and soil moisture availability, complex

dynamics in isotopic composition will emerge and propagate through the plant. The above hypothesis, if true, would make the comparison of isotopic data among individuals, species, and studies difficult.

In this study, we provide a critical assessment of the assumption of δ_{xyl} invariance along the length of woody plant stems and over short time periods. We first show that variation in δ_{xyl} along the length of lignified plants exceeds the expected measurement error using three independent datasets including i) canopy trees and lianas sampled at different heights in French Guiana; and ii) plant species from northwestern China (Zhao *et al.*, 2014) and iii) European Beech and Silver firs in south-west Germany (Magh *et al.*, 2020). Second, we build a simple mechanistic model that incorporates basic plant hydraulic transport processes. The model predicts that diurnal changes in water potential gradient between soil and roots result in shifting sources of water absorption that differ in their isotope composition.

2. Materials and Methods

2.1. Part A: Empirical exploration

2.1.1. Field data French Guiana: variation in δ_{xyl} with plant height

Six canopy trees and six canopy lianas were sampled during two subsequent dry days (24-25 August 2017) at the Laussat Conservation Area in Northwestern French Guiana (05°28.604'N-053°34.250'W). Stem xylem tissue of individual plants was sampled at different heights (1.3, 5, 10, 15 and 20 m where possible) at the same radial position of the stem, between 9:00 and 15:00. Stem samples were stripped off bark and phloem tissues. Soil samples were collected at different depths (0.05, 0.15, 0.30, 0.45, 0.60, 0.90, 1.20, and 1.80m) with a soil auger and in close vicinity to the sampled individuals. Samples were placed in glass collection vials, sealed with a cap, and frozen awaiting cryogenic vacuum distillation (CVD; 4 h at 105°C). When the

weight loss of a sample resulting from the extraction process was below 98%, the sample was excluded (after Araguás-Araguás *et al.*, 1998) (see Fig S1).

The isotope composition of the water in the samples was measured with a Wavelength-Scanned-Cavity Ring-Down Spectrometer (WS-CRDS, L2120-i, Picarro, California, USA) coupled with a vaporizing module (A0211 High Precision Vaporizer) and a micro combustion module to avoid organic contamination (Martin-Gomez et al., 2015; Evaristo et al., 2016). Post-processing of raw δ-readings into calibrated δ-values (in ‰, V-SMOW) was performed using SICalib (version 2.16; Gröning, 2011). More details on the sampling site and sampling procedure can be found in supplementary methods A.

2.1.2. Field data China: temporal variation in δ_{xyl}

Plant δ_{xyl} was sampled at high temporal resolution in the Heihe River Basin (HRB), northwestern China. Four distinct study locations differing in altitude, climatological conditions, and ecosystem types were selected. At each location, the dominant tree, shrub, and/or herb species were considered for sampling. In August 2009, *Populus euphratica* was sampled in the Qidaoqiao riparian forest (42°01'N-101°14'E) and *Reaumuria soongorica* in the Gobi desert ecosystem (42°16'N-101°17'E; 906-930 m a.s.l). In June–September 2011 *Picea crassifolia*, *Potentilla fruticose*, *Polygonum viviparum* and *Stipa capillata* were measured in the Pailugou forest ecosystem (38°33'N-100°18'E; 2700-2900 m a.s.l). All species were sampled every 2-hours over multiple days (3-4), except for *P. crassifolia*, which was measured hourly. Stem samples were collected for trees and shrubs, while root samples were obtained for the herb species. More details are available in Zhao *et al.* (2014).

Upon collection, all samples were placed in 8 mL collection bottles and frozen in the field stations before transportation to the laboratory for water extraction via CVD (Zhao *et al.*, 2011). Both $\delta^{18}O$ and $\delta^{2}H$ were assessed with an Euro EA3000 element analyzer (Eurovector,

Milan, Italy) coupled to an Isoprime isotope ratio mass spectrometer (Isoprime Ltd, UK) at the Heihe Key Laboratory of Ecohydrology and River Basin Science, Cold and Arid Regions Environmental and Engineering Research Institute. Internal laboratory references were used for calibration, resulting in measurement precision of ±0.2‰ and ±1.0 ‰ for $\delta^{18}O$ and $\delta^{2}H$, respectively.

2.1.3. Field data Germany: high temporal variation in δ_{xyl}

A δ_{xyl} monitoring campaign, studying mature Silver firs (*Abies alba*; n=3) and European beeches (*Fagus sylvatica*; n=3), was conducted during progressing drought conditions (6-11 July 2017) at the "Freiamt" field site in south-west Germany. Isotopic composition of xylem water was obtained from branch samples, which were collected every two hours between 7:00 and 21:00 at the same height and canopy orientation in the sun crown. Branches were stripped of bark and phloem tissue. A Scholander Pressure chamber (Scholander, 1966), which allowed concomitant registration of water potential of the sampled branches, was used to extract xylem water directly in the field (Rennenberg *et al.*, 1996). Both $\delta^{18}O$ and $\delta^{2}H$ of branch samples were determined with a wavelength scanned cavity ring-down spectrometer (Picarro L2130i, Santa Clara, USA), followed by data correction using ChemCorrect™ (Picarro, 2010). For more details see Magh *et al.* (2020).

2.1.4. Field data normalization

To aid visual comparisons, we use normalized δ_{xyl} values ($\beta^2 H_X$ and $\beta^{18} O_X$) which describe the deviation of an individual sample from the average isotopic composition (a) along the height *h* of the stem, or (b) over one day:

$$\beta^2 H_X = \delta^2 H_X - \frac{1}{N}\sum_{j=1}^{N} \delta^2 H_{X,j} \qquad \text{Eq. (1)}$$

With *N* the number of sampled heights or time steps during one day.

2.2. Part B: Model exploration

2.2.1. Model derivation

The expected δ_{xyl} at different stem heights within a tree during the course of the day can be derived from plant and physical properties such as root length density, total fine root surface area, water potential gradients, and the isotope composition of soil water (Fig. 2). We call this the SWIFT model (i.e. Stable Water Isotopic Fluctuation within Trees). To derive the SWIFT model, we first describe the establishment of δ_{xyl} entering the tree at the stem base via a multi-source mixing model (Phillips & Gregg, 2003). We subsequently consider vertical water transport within the tree, which relates to the established sap flow pattern.

To ensure consistency and clarity in variable declarations we maintain the following notation in the subscripts of variables: uppercase roman to distinguish the medium through which water travels (X for xylem, R for root, S for soil) and lowercase for units of time and distance (h for stem height, t for time and i for soil layer index). A comprehensive list of variables, definitions, and units is given in Table 1. A schematic representation of the model is provided in Fig. 2a. Note that the model presented here focuses on hydrogen isotopes (i.e. $^{2}H/^{1}H$) but can easily be used to study oxygen isotopes (i.e. $^{18}O/^{16}O$).

i. Isotope composition of plant xylem water at stem base.

The $\delta^{2}H$ composition of xylem water of an individual plant at stem base ($\delta^{2}H_{X,0,t}$) (i.e. height zero; h = 0m; Fig. 2a) at time t, can theoretically be derived by calculating a weighted average of water taken up from different soil depths (Phillips & Gregg, 2003). The root zone is divided into n discrete soil layers of equivalent thickness Δz. Here, we assume a constant $\delta^{2}H$ composition of soil water ($\delta^{2}H_{S,i}$) over time in each soil layer, a reasonable assumption when

isotopic measurements are conducted during rain-free periods, allowing the expression of $\delta^2 H_{X,0,t}$ as:

$$\delta^2 H_{X,0,t} = \sum_{i=1}^{n} f_{i,t} \cdot \delta^2 H_{S,i} \quad \text{Eq. (2)}$$

where $f_{i,t}$ is the fraction of water taken up at the i^{th} soil layer (Fig. 2a) defined as:

$$f_{i,t} = \frac{RWU_{i,t}}{\sum_{i=1}^{n} RWU_{i,t}} \quad \text{Eq. (3)}$$

and $RWU_{i,t}$ is the net amount of water entering and leaving the roots at time *t* in the i^{th} soil layer ($RWU_{i,t}$ is defined positive when entering the root). The current representation of the model does not account for water loss via the root system nor for mixing of the extracted water from different soil layers within the roots until the water enters the stem base. When tree capacitance is neglected, the sum of $RWU_{i,t}$ across the entire root zone is equal to the instantaneous sap flow at time *t*, SF_t:

$$SF_t = \sum_{i=1}^{n} RWU_{i,t} = \sum_{i=1}^{n} -k_i \cdot A_{R,i} \cdot \left[\Psi_{X,0,t} - (\Psi_{S,i,t} - z_i)\right] \quad \text{Eq. (4)}$$

Where k_i is the plant-specific total soil-to-root conductance over soil layer *i*, $\Psi_{X,0,t}$ is the water potential (i.e. the hydraulic head) at the base of the plant stem and $\Psi_{S,i,t}$ is the soil matric potential at the i^{th} soil layer (Fig. 2a). Total plant water potential is generally defined as the sum of the solute, pressure, gravity, and matric potential. As long-distance water transport through the xylem is studied, the osmotic potential and the kinetic energy head can be assumed negligible (Früh & Kurth, 1999). The xylem pressure potential is represented as $\Psi_{X,0,t}$. And the term z_i is the gravimetric water potential necessary to lift the water from depth z_i to the base of the stem, assuming a hydrostatic gradient in the transporting roots. The model considers z_i to be a positive value (zero at the surface), thus z_i is subtracted $\Psi_{S,i,t}$. $A_{R,i}$ is the absorptive root area distribution over soil layer *i* (Fig. 2a). This parameter $A_{R,i}$ can be derived from plant

allometric relations with stem diameter (Čermák *et al.*, 2006), and subsequently distributed over the different soil layers, considering the power-law distribution of Jackson *et al.* (1995).

The total soil-to-root conductance is calculated assuming the root and soil resistances are connected in series (Fig. 2a):

$$k_i = \frac{k_R \cdot k_S}{k_R + k_S} \quad \text{Eq. (5)}$$

where k_R is the effective root radial conductivity (assumed constant and uniform), and $k_S = K_{S,i}/\ell$ is the conductance associated with the radial water flow between soil and root surface. $\ell = 0.53/\sqrt{\pi \cdot B_i}$ represents the effective radial pathway length of water flow between bulk soil and root surface (De Jong van Lier *et al.*, 2008; Vogel *et al.*, 2013) with B_i giving the overall root length density distribution per unit of soil. $K_{S,i}$ is the soil hydraulic conductivity for each soil depth. $K_{S,i}$ depends on soil water moisture and thus relates to the soil matric potential $\Psi_{S,i,t}$ of the soil layer where the water is extracted. $K_{S,i}$ is computed using the Clapp & Hornberger (1978) formulation:

$$K_{S,i} = K_{s,max} \cdot \left(\frac{\Psi_{sat}}{\Psi_{S,i,t}}\right)^{2+\frac{3}{b}} \quad \text{Eq. (6)}$$

where $K_{s,max}$ is the soil conductivity at saturation and b and Ψ_{sat} are empirical constants that depend on soil type (here considered as constant over all soil layers).

Subsequently, $f_{i.t}$ can be restructured as:

$$f_{i.t} = \frac{k_i \cdot A_{R,i} \cdot \Delta\Psi_{i,t}}{\sum_{i=1}^{n} k_i \cdot A_{R,i} \cdot \Delta\Psi_{i,t}} \quad \text{Eq. (7)}$$

where the root water to soil matric potential gradient is represented as $\Delta\Psi_{i,t} = \Psi_{X,0,t} - (\Psi_{S,i,t} - z_i)$.

Combining Eq. (2) and Eq. (7) then allows the derivation of $\delta^2 H_{X,0,t}$ as follows:

$$\delta^2 H_{X,0,t} = \sum_{i=1}^{n} \left(\frac{k_i \cdot A_{R,i} \cdot \Delta\Psi_{i,t}}{\sum_{j=1}^{n} k_j \cdot A_{R,j} \cdot \Delta\Psi_{j,t}} \cdot \delta^2 H_{S,i} \right) \quad \text{Eq. (8)}$$

This equation requires estimates of $\Delta\Psi_{i,t}$, which is preferably measured instantaneously in the field (i.e. via stem and soil psychrometers for $\Psi_{X,0,t}$ and $\Psi_{S,i,t}$, respectively). However, as measurements of $\Psi_{X,0,t}$ are not always available, estimated $\widehat{\Psi}_{X,0,t}$ can be derived from sap flow by re-organizing Eq. (4) into:

$$\widehat{\Psi}_{X,0,t} = \frac{\sum_{i=1}^{n} [k_i \cdot A_{R,i} \cdot (\Psi_{S,i,t} - z_i)] - SF_t}{\sum_{i=1}^{n} k_i \cdot A_{R,i}} \quad \text{Eq. (9)}$$

which then allows replacement of $\Psi_{X,0,t}$ with $\widehat{\Psi}_{X,0,t}$ in Eq. (8).

ii. Height-dependent isotope composition of plant xylem water

In our model, the water isotopologues simply move upwards from the stem base with the sap flow velocity. Assuming negligible diffusion, the δ^2H isotope composition in xylem water at height *h* and time *t* ($\delta^2 H_{X,h,t}$) is then the isotope composition of xylem water at stem base at time $t - \tau$.

$$\delta^2 H_{X,h,t} = \delta^2 H_{X,0,t-\tau} \quad \text{Eq. (10)}$$

where τ is the lag before $\delta^2 H_{X,0,t}$ reaches stem height *h* (Fig. 2a), which depends on the true sap flux density in the xylem (SF_V). True sap flux density indicates the real speed of vertical water displacement within a plant, derived by dividing SF_t over the lumen area of the plant (A_x; Fig. 2a) i.e. the total cross-sectional area of the vessels. τ can be obtained from the mass conservation equality:

$$h \cdot A_x = \int_{t-\tau}^{t} SF_t \, dt \quad \text{Eq. (11)}$$

Note that since most scientific studies express sap flux density as the sap flow over the total sapwood area (SF_S), rather than over the total vessel lumen area (SF_V), for consistency, we will present the model outputs as functions of SF_S.

Note that SF_V presents the sap flux density normalized over the total vessel lumen area, and as vessel lumen area correlates with plant diameter at breast height (DBH), there is no need for explicit consideration of DBH in the model for comparison among field measurements.

Model analyses show that the impact of the mutual diffusion coefficient of heavy water in normal water on the transport flux is negligible for plants with high sap flux densities, which is the case for the theoretical examples below. However, in plants with low sap flow densities, consideration of diffusion might be required. Diffusion might also be generated by water passing through a complex network of vessels, in analogy to diffusion in a porous media (see supplementary methods B for some analytical results, simulated cases of and a detailed discussion on the role of diffusion). SWIFT was implemented in R version 3.4.0 (R Core Team, 2017), and is publicly available (see GitHub repository HannesDeDeurwaerder/SWIFT).

iii. Model parameterization and analyses

The model's primary purpose is to gain insight into 1) which processes are capable of generating δ_{xyl} variance, and 2) how sensitive the variance in δ_{xyl} along the stem is in response to the modeled plant hydraulic processes. To this end, we adopted the basic plant parameters from Huang *et al.* (2017) who studied soil-plant hydrodynamics of loblolly pine (*Pinus taeda L.*) during a 30-day extended dry down period (Table S1). We started with synthetic basal sap flow patterns and volumes extracted from the model runs of Huang *et al.* (2017) for a typical drought day (day 11). Both basal sap flow patterns and volumes are repeated over the studied period, as no variation between days is assumed. Sap flow follows the plant's water demand which is the result of daily cycles of transpiration driven by photosynthetic active solar radiation

(PAR), vapor pressure deficit (VPD), and optimal stomatal response (Epila *et al.*, 2017). Secondly, both the soil matric potential ($\Psi_{S,i,t}$) and δ^2H composition of soil water ($\delta^2 H_{S,i}$) profiles with soil depth were adopted from Meißner *et al.* (2012) (Fig. S8, see Table S1 for equations) as driver data of the model, and were assumed to stay constant over time. Since measurements of Meißner *et al.* (2012) were conducted at a silt loam plot in the temperate climate of central Germany, corresponding soil parameters were selected from Clapp & Hornberger (1978). Subsequently, the following model simulations were executed (see Fig. 2a):

1) **Analysis A1: impact of temporal SF_t variation on the isotope composition of xylem water at a fixed stem height.** Temporal patterns in δ^2H isotope composition in xylem water ($\delta^2 H_X$) were evaluated for a typical situation, i.e. measurement at breast height (h=1.30 m) (e.g. White *et al.*, 1985; Meinzer *et al.*, 1999; Goldsmith *et al.*, 2012; Hervé-Fernández *et al.*, 2016; De Deurwaerder *et al.*, 2018; Muñoz-Villers *et al.*, 2019).
2) **Analysis A2: impact of temporal SF_t variation at different tree heights.** Temporal patterns in $\delta^2 H_X$ within a tree at various sampling heights (5, 10, and 15 m).
3) **Analysis A3: impact of temporal SF_t variation on the isotope composition of xylem water and the timing of sampling.** Representation of the profile of $\delta^2 H_X$ along the full height of a tree, measured at different sampling times (9:00 and11:00), with the standard parameterization given in Table S1.
4) **Analysis B: variation in $\delta^2 H_X$ due to differences in absolute daily average sap flow speed.** Diurnal patterns in the $\delta^2 H_X$ in trees that differ solely in daily averaged SF_V, which are set to 0.64, 0.42, and 0.19 m h^{-1}, respectively corresponding to SF_S values of 0.09, 0.06 and 0.03 m h^{-1}.

All parameters of the four analyses are given in Table S1. The model simulations for each analysis were compared to a null model.

iv. The null model

The null model adopts the standard assumption of zero variation in δ_{Xyl} along the length of the plant body, but allows for potential measurement errors related to the extraction protocol. In reality, empirically obtained data will have some variation as observed values ($Obs.\,\delta_{Xyl}$) are the sum of the true δ_{Xyl}-values and their extraction error ($error_{extraction}$).

$$Obs.\,\delta_{Xyl} = True\ \delta_{Xyl} + error_{extraction} \quad \text{(eq. 12)}$$

Hence, the null model attributes any variance in isotopic composition to extraction errors, with maximum extraction error ranges of 3‰ for δ^2H samples (0.3‰ for $\delta^{18}O$) expected for water extraction recovery rates higher than 98% (e.g. Orlowski *et al.*, 2013). These extraction errors are negatively skewed following the Rayleigh distillation model, which predicts that extraction error for incomplete water recovery will be negative, and therefore Obs. $\delta_{xyl} \leq$ True δ_{xyl}. The null model represents this $error_{extraction}$ by a negative skew-normal distribution (with location parameter ξ = 0‰, the scale ω = 3‰ for δ^2H or 0.3‰ for $\delta^{18}O$, and shape α = -∞) (Azzalini, 2013).

2.2.2. Estimation of average RWU depth

Average RWU depths (i.e. the weighted mean of the depths of RWU, with the uptake fractions at the different depths as weights) were derived from the simulated δ^2H_X values by use of both the direct inference method and the end-member mixing analysis method. Together, these techniques represent 96% of the applied methods in the literature (Rothfuss & Javaux, 2017), and the reader is referred to Rothfuss & Javaux (2017) for a complete discussion of both

techniques. In line with the general approach assessing RWU with stable water isotopes, the average RWU depth is obtained by relating the δ^2H_X with the $\delta^2H_{S,i}$ depth profile. We compared average RWU depth estimates obtained from simulated δ^2H_X, as described in the analyses above, with the true average RWU depth. Here, the true average RWU depth was defined as the depth corresponding to the daily weighted average δ^2H_X, calculated as the weighted sum of $\delta^2H_{X,i,t}$ and the relative fraction of water taken up at each depth.

2.2.3. Transport dynamics and sensitivity analysis

We perform a basic model validation of our model assumption that the propagation of an isotopic signature is driven by diurnal sap flow dynamics and diffusion alone. In essence, the model assumes that once water with a given isotopic signature enters the stem, it moves upwards with the speed of sap flow, and changes only due to the effect of diffusion. The effects of capacitance on δ^2H_X dynamics by the release of storage water in the xylem flow can be ignored. To validate this assumption we compare model predictions against observed δ^2H_X dynamics monitored within a pine tree (*Pinus pinea L.*) following ^2H-enrichment in a controlled greenhouse experiment, as detailed in Marshall *et al.* (2020). δ^2H_X was measured at two heights (0.15 and 0.65m) using a novel *in situ* technique, the borehole equilibration method. Performed model simulations consider the absolute ranges of sap flux densities during the entire monitoring campaign, with the account of tree tapering effect on sap flux densities over the studied stem length (supplementary method C). Validation of diurnal variation in δ^2H_X requires high temporal resolution monitoring of δ^2H_X dynamics in plants stems, with simultaneous high temporal resolution monitoring and characterization of sap flow, soil water potential, and isotopic composition. Such data does not yet exist to our best of knowledge.

In addition, we performed two sensitivity analyses to assess the relative importance of each parameter in generating variance in δ^2H_X along the length of a plant. In both sensitivity analyses,

we varied model parameters one-at-a-time to assess the local sensitivity of the model outputs for soil type, sap flux density, root properties, and sampling strategies. The sensitivity analysis provides insight into possibilities for improving the design of field protocols, by revealing potential key measurements and caveats in field setups. More details on the performed sensitivity analysis and validation of transport dynamics are available in supplementary method C.

3. Results

3.1. Part A: Empirical exploration

The null model assumes constant isotopic composition of root water uptake, with only limited variance in isotopic composition introduced by extraction errors ($\beta^2 H_X < 3‰$; $\delta^{18}O_X < 0.3‰$). However, pronounced $\delta^2 H_X$ variance within individual plants, exceeding the null model ranges, are observed in all three independent datasets. The normalized $\delta^2 H$ composition in xylem water ($\beta^2 H_X$) along the stem length of lianas and trees in French Guiana exceeded the null model by a factor of 3.2 and 4.3, respectively (Fig. 3c, Fig. S2). Differences up to 13.1‰ and 18.3‰ in $\delta^2 H$ and 1.3‰ and 2.2‰ in $\delta^{18}O$ were observed in individuals of trees and lianas, respectively (Supplementary method A, table A,).

Similarly, diurnal intra-individual $\delta^2 H_X$ variances were found for all considered plant growth forms, i.e. trees, shrubs, and herbs, monitored in China (Fig. 4b-d, Fig S3). Observed daily maximum differences in $\delta^2 H_X$ were 18.0‰, 21.0‰, and 25.2‰ for trees, shrubs and herbs respectively (2.8‰, 6.8‰, and 6.5‰ in $\delta^{18}O_X$ in Fig. S4). The expected null model variance was exceeded for each species during its measurement period.

Finally, pronounced intra-individual $\delta^2 H_X$ variance was also observed for all monitored firs and beeches in Germany (Fig 4e, Fig. S5). Here, daily maxima differences in $\delta^2 H_X$ were 8.2

‰ and 14.2 ‰ for *Abies alba* and *Fagus sylvatica* respectively (2.0‰ and 4.2 ‰ in $\delta^{18}O_X$ in Fig. S6).

3.2. Part B: Model exploration

Isotope composition of xylem water at stem base and basic model behavior

At the stem base, simulated $\delta^2H_{X,0,t}$ displays a diurnal fluctuation (Fig. 2b, Fig S7) that corresponds to the daily sap flow pattern (Fig. S7). This pattern is caused by shifting diurnal average RWU depth. Early in the morning, when transpiration is low, most of the RWU occurs in deeper layers, where soil matric potential is less negative and where soil water is more depleted in ^2H compared with the soil layers above (Fig. S8a-b). As transpiration increases during the day, a significant proportion of RWU can now be extracted from the drier, shallower layers, where the soil water is enriched in ^2H, i.e., having a higher δ^2H. In the afternoon, as transpiration declines, the isotopic composition reflects again the composition of the more depleted soil water in the deeper soil layers, and it remains constant throughout the night because apart from diffusion SWIFT does not consider mixing of the internal stem water. The mixing effects of diffusion are only noticeable at low sap flow speeds (Fig. 3b).

Highest δ^2H_X-values (approx.-59‰) are found in alignment with the diurnal minimum of $\Psi_{X,0,t}$ (approx.-0.85 MPa, Fig. S7). At this moment, the difference between $\Psi_{X,0,t}$ and $\Psi_{S,i,t}$ is maximal, enabling water extraction from the upper and driest soil layers. Most root biomass is located near the surface (cf. Jackson *et al.*, 1995; Fig. S8c) and uptake in these layers will result in relatively high contributions to the total RWU.

In contrast, differences between $\Psi_{X,0,t}$ and $\Psi_{S,i,t}$ are smaller in the early morning and late afternoon causing root water uptake in the upper soil layers to halt. The decreasing in absolute range of $\Delta\Psi_{i,t}$ translates into higher proportions of RWU originating from deeper, more

411 depleted soil layers. This causes δ^2H_X to drop to a baseline of approx. -67‰. This afternoon
412 depletion of δ^2H_X will henceforth be referred to as the δ^2H_X-baseline drop.

413 *Isotope composition of xylem water at different times, heights and SF_V*

414 Temporal fluctuation in δ^2H_X within a tree at 1.3 m (i.e. the standard sampling height;
415 Analysis A1; Fig. 2a) and other potential sampling heights (e.g. branch collection; Analysis A2;
416 Fig. 2a), are provided in Fig. 2b and 3a. Both analyses show that fluctuations in δ^2H_X depend
417 on the height of measurement and the corresponding time needed to move the water along the
418 xylem conduits. Note that it depends on the selected temporal resolution whether the δ^2H_X-
419 baseline drop at a given height equals the (stem base) minimum (here 1 min, see Fig. S12). In
420 addition to sampling height, analysis A3 depicts the importance of sampling time (Fig. 3a).
421 Outputs of analysis B predict that the occurrence and width of the δ^2H_X-baseline drop are a
422 function of the sap flow velocity SF_V (Fig. 3b). To aid model interpretation and comparability
423 with field data, we (i) provide an illustrative example of normalized δ^2H isotope composition
424 of model-simulated xylem water (β^2H_X) with consideration of extraction error (Fig. 4a), and (ii)
425 display the relation between δ^2H_X variance and cumulative sap flow volumes, for which the
426 piston flow dynamics in SWIFT originate from lateral translation of the δ^2H_X fluctuation at
427 $\delta^2H_{X,0,t}$ (Fig. 2b).

428

429 **3.2.1. Potential biases in average RWU depth estimation**

430 Both timing of measurement (Fig. 5a) and SF_V (Fig. 5b) influence average RWU depth
431 estimates derived via the direct inference and end-member mixing analysis method (Fig. S9).
432 Collection of tree samples at 1.30 m can result in erroneous estimation, deviating up to 104 %
433 from the average daily RWU depth (Fig. 5). Plotting the relative error in average RWU depth
434 as a function of time and SF_V (Fig. 5) shows that it is possible to time δ^2H_X measurements in a

fashion that captures unbiased estimates of the average RWU depth. Xylem water sampling should be timed to capture the δ^2H_X that corresponds to water extracted at peak RWU, and the expected sampling time can be derived by considering the time needed for the water to reach the point of measurement (i.e. at 1.30 m in Fig. 5).

3.2.2. Transport dynamics and sensitivity analysis

Our sensitivity analyses show that the expected absolute error in average RWU depth assessment is directly related to both 1) maximum variance in and 2) the probability of sampling non-representative δ^2H_X values. The maximum variance depends on the height, while the probability of sampling non-representative areas depends on the width of the "δ^2H_X-baseline drop" respectively (defined above). Hence, variation in δ^2H_X is determined by several factors, including the sampling strategy (timing and height of sampling), sap flow velocity (Fig. S10), and below-ground biophysical parameter (Fig. S11). We summarized the most important variables as predicted by SWIFT, which should be considered in subsequent RWU studies.

Plants on loamy soils show larger diurnal δ^2H_X variances in comparison with those on clay soils for a similar prevailing isotope gradient across the soil profile. Larger variances correspond to potentially larger errors, but the steeper slope of the δ^2H_X curve results in a thinner δ^2H_X-baseline drop. Hence, loamy soil can result in potentially the large error but this is mediated by a lower probability of sampling non-representative δ^2H_X values during the day.

The volume of water taken up by the plant (SF_t; Fig. S11b) affects xylem water potential of the plant at stem base ($\widehat{\Psi}_{X,0,t}$). Higher SF_t requires more negative $\widehat{\Psi}_{X,0,t}$, enabling the plant to access the enriched soil water of more shallow soil layers. Therefore, an increase in SF_t results in the increase of maximum δ^2H_X values (increased maximum error) but also results in

458 a smaller width of the baseline drop (Fig. 2-3). Lower SF_t result in smaller errors, but a larger
459 probability of sampling a non-representative area (Fig. 3b).

460 Root properties, i.e. root membrane permeability (Fig. S11c) strongly influence both the
461 total range of δ^2H_X variance and the width of the δ^2H_X-baseline drops. Decreasing root
462 membrane permeability, but with no alterations to the sap flow volumes, results in thinner δ^2H_X-
463 baseline drops, but higher maximum δ^2H_X variance.

464 In addition, the true sap flow velocity (SF_t per unit of lumen area) will determine the relative
465 importance of diffusion on the δ^2H_X dynamics. Diffusion can cause a smoothing of the peak and
466 a consequent increase in the width of the δ^2H_X-baseline drop. However, as diffusion is
467 proportional to the time that water isotopologues remain in the xylem, its absolute impact on
468 δ^2H_X is negligible in plants with a high true sap flow velocity. In contrast, the impact of diffusion
469 on δ^2H_X dynamics is substantial for plants with very low velocities, where water takes many
470 days to pass from roots to leaves (see supplementary method B).

471 The role of diffusion was investigated using a stepwise ^2H enrichment experiment in Marshall *et al.*
472 (2020) (Fig 6). Analytical solutions of an advection-diffusion equation show that at 0.15 cm, a relatively
473 small diffusivity was required to reproduce the initial increase of xylem isotope signature, with values
474 comparable to these reported for diffusivity of heavy water (Meng *et al.*, 2018). However, at 65 cm, the
475 value of diffusivity required to match the observed initial increase was much higher, suggesting other
476 processes besides molecular diffusivity might contribute to the isotope transport (e.g. variable flow
477 velocities within vessels and among vessels of the xylem network). Note also that the analytical solutions
478 were not able to recover the second part of the curve where the isotope reaches the asymptotic enriched
479 value, which is more gradual in the observations (Fig. 6). This also suggests a complex transport of δ^2H_X
480 in the xylem.

481

482 ## 4. Discussion

4.1. Dynamic diurnal isotope compositions of xylem water along plant stems

Empirical field data show pronounced δ_{xyl} variance along the stem length (Fig. 3) and over a sub-daily time period (Fig. 4). Our model explorations suggest that basic plant hydraulic functioning can result in shifting mixtures of δ^2H_X entering the plant (Fig. 2-3). Daily $\Psi_{X,0,t}$ fluctuations interact with the $\Psi_{S,i,t}$ profile causing different parts of the root distribution to be active during the day. The fluctuations in δ^2H_X at the stem base propagate along the xylem with a velocity proportional to the sap flow and this produces variability in sampled δ^2H_X that is much larger than the expected measuring error. Consequently, rather than being static, δ^2H_X values along the height of a plant should be envisioned as a dynamic diurnal process.

Importantly, we show that high variance in δ^2H_X can result in an incorrect assessment of differences in average RWU depths between plants. Differences do not necessarily result from variability in average RWU depth, but may result from monitoring plants at different heights (Fig. 2-3), at different times (Fig. 3a) or by comparing individuals which have different SF_V (Fig. 3b) and xylem anatomical properties. For example, depending on SF_V and lumen area, the isotopic signal can take hours or days to travel from roots to leaves - as was also observed experimentally (Steppe *et al.*, 2010; Magh *et al.*, 2020; Marshall *et al.*, 2020).

Low SF_V allows multiple δ^2H_X-baseline drops over the length of a single tree. Sampled δ^2H_X can reflect soil isotopic composition of the past several days. Our sensitivity analysis reveals that various soil and plant characteristics have an important role in determining both the daily maximum δ^2H_X variance as well as the width of the δ^2H_X -baseline drop. These two characteristics directly impact (i) the expected maximum bias in estimates of average RWU depth and (ii) the chance of measuring δ^2H_X values that do not represent a mixture of all rooting layers during peak RWU (i.e. measurements in the baseline drop). Ultimately, these factors will challenge the use of stable water isotope to study the terrestrial water fluxes as recently

reviewed by Penna *et al.* (2018). We additionally advocate that future research should explore the minimum set of (bio)physiological drivers and processes that require quantification to correctly interpret δ^2H_X along the hydraulic pathway length of a plant.

4.2. General applicability of model and results

A necessary condition for diurnal shifts in RWU is the existence of water potential differences, e.g. more negative water potentials in the upper layers where trees usually have higher root density, which can cause a disproportional partitioning of diurnal RWU between deep and shallow roots over a diurnal course. The pronounced variance in δ_{xyl} identified in this study is intrinsic to the isotopic tracing technique for RWU assessment, as this method relies on the existence of a soil water isotopic profile. Such profiles are the result of soil evaporation, a process inextricably coupled to water potential heterogeneity, and hence to variance in δ^2H_X.

Plant transpiration results from a complex interaction between atmospheric demands (i.e. driven by VPD and radiation) and stomatal conductance that depends on tolerance for drought stress and soil moisture content. We may expect diurnal fluctuation in radiation and VPD, and hence in water transport and depth of water absorption, as modeled here to be a general phenomenon in nature. Moreover, much greater fluctuations in VPD and radiation should be expected under natural conditions than the diurnal cycle described here, and these will increase the variability of transpiration fluxes, leading to even more complex dynamics of $\Psi_{X,0,t}$. Specifically, the model simulations suggest that intra-individual variability of δ^2H_X will reflect the past changes of RWU dynamics, including RWU dynamics driven by changes of environmental demands. For instance, a changing degree in cloud cover that impacts sap flow dynamics can influence $\Psi_{X,0,t}$ rather abruptly (e.g. in lianas; Chen *et al.*, 2015) and lead to

instantaneous changes in the δ^2H composition of the water mixture taken up at the root level. This can complicate the comparison of different plants sampled at different heights and times.

Note that, based on our model, we expect that soil isotopic enrichment experiments will generate extensive δ^2H_X variation along the length of trees whenever diurnal RWU fluctuations cause water extraction to shift between labeled and unlabeled soil layers. Furthermore, when enrichment experiments target trees with different hydraulic properties (such as SF_V) care should be taken to determine when and where to sample these trees to assess a potential ^2H enrichment in xylem water (Fig. 6, but see Magh *et al.*, 2020;).

4.3. Alternative causes of δ_{xyl} fluctuation

The SWIFT model provides a simple traceable and mechanistic explanation, using diurnal variations in SF_t and RWU, for the pronounced variance and dynamic nature of the δ_{xyl} fluctuations with plant height and time of field samples (e.g. Fig. 3-4) and elsewhere (Cooper *et al.* 1991). However, several other processes might contribute to generate variability, while others can act to damp this variability. In the next section, we will discuss alternative causes, complementary and antagonistic, that contribute to the observed intra-individual δ_{xyl} variances.

i. Fractionation at root or stem level

An increasing body of observations shows the occurrence of isotopic fractionation at the root level governed by root membrane transport (Lin & Sternberg, 1993; Vargas *et al.*, 2017) or by unknown reasons (Zhao *et al.*, 2016). Brinkmann *et al.* (2019) hypothesize that root level fractionation causes disparity when average RWU depth calculations based on δ^2H_X measurements are compared with those of $\delta^{18}O_X$. However, it is difficult to imagine a scenario where root fractionation by itself can explain the observed diurnal fluctuations in δ_{xyl} with height and time. Even if root fractionation significantly contributed to variation in δ_{xyl}, we

554 would still need to take into account diurnal fluctuation in RWU to explain the observed
555 patterns. Isotopic enrichment of xylem water along the stem length was observed in association
556 with stem transpiration (Dawson & Ehleringer, 1993; Barnard *et al.*, 2006). However, this
557 phenomenon is generally restricted to non-suberized plants and in woody branches in close
558 vicinity to the evaporative surface of the plant (Dawson & Ehleringer, 1993). Isotopic
559 enrichment can, therefore, not explain the variances in δ_{xyl} observed in our empirical data, which
560 were sampled within the main stem (data French Guiana) or from lignified branch segment
561 distant from evaporative surfaces (data China and Germany).

562 ii. *Temporal and spatial soil dynamics*

563 Soil water content can be extremely heterogeneous in the three spatial dimensions as well
564 as in time with complex dynamics of soil water movement. For example, hydraulic lift vertically
565 redistributes soil water through the roots (Dawson & Ehleringer, 1993), which may change the
566 water isotopic composition of the water mixture in the rhizosphere that is taken up by roots.
567 Specifically, hydraulic lift redistributes and mixes the isotopic signal of depleted soil water in
568 deeper layers with the enriched soil water signal in the rhizosphere in shallower layers. This
569 should lead to lower variation in the soil water accessible to the plant, and hence less variation
570 along plant height. Horizontal heterogeneity of water content may also affect δ_{xyl} variance as
571 soil water potentials and the isotope composition of soil water are interlinked. Under these
572 conditions, it is important to understand how much the radial distribution of roots will naturally
573 average out soil heterogeneity. However, note that heterogeneity in the soil does not
574 automatically translate in variability in the xylem. Differential root water uptake driven by the
575 diurnal fluctuation in water potential gradients in the soil-plant interface is still required to
576 generate variability in the xylem isotopic signature.

577 *iii. Storage tissue and phloem enrichment*

578 Storage tissues release water and sugars into the xylem conduits on a daily basis to support
579 water transpiration demand (Goldstein et al., 1998; Morris et al., 2016; Secchi et al., 2017) or
580 to repair embolism (Salleo et al., 2009; Secchi et al., 2017). Both water and sugars are
581 transported in and out of storage tissue via symplastic pathways using plasmodesmata and
582 aquaporins (Knipfer et al., 2016; Secchi et al., 2017), a pathway that has been linked to isotopic
583 fractionation in roots (Ellsworth & Williams, 2007). Moreover, phloem transports
584 photosynthetic assimilates that were produced in the leaves and are therefore potentially
585 affected by transpiration fractionation (Gessler *et al.*, 2013). Hence, these metabolic molecules
586 might show higher values of δ^2H and $\delta^{18}O$ compared to RWU. Water release from storage or
587 phloem tissue might locally alter δ_{xyl} (White et al., 1985). Additionally, the time between water
588 storage and release could bridge multiple days, and corresponding isotopic composition may
589 reflect soil conditions antecedent a dry spell when the isotopic signature of soil was less
590 vertically stratified. It is evident that such dynamics are complex, and it is hard to predict how
591 storage tissue and phloem enrichment affect observed δ_{xyl} patterns. Importantly, xylem isotopic
592 sampling cannot differentiate between water resulting from RWU or storage, and therefore we
593 cannot exclude the possibility that tissue and phloem enrichment play a role. At a minimum this
594 adds further uncertainty to RWU assessment. Water derived from storage tissues might also be
595 present in larger fraction in higher parts of the plants, especially branches, as contamination
596 accumulates as water moves upwards.

597 Unfortunately, to our best knowledge, empirical data on the isotopic composition of storage
598 tissue and its spatiotemporal dynamics are absent in the literature. Future research should target
599 impact assessment of storage water on intra-individual δ_{xyl}, allowing proper implementation in
600 the model.

601 *Diffusion processes*

Diffusion is a process of net movement of molecules from a region of higher concentration to a region of lower concentration. Consequently, diffusion dampens δ_{xyl} variability, both in time and space within water xylem. Although the mutual diffusion coefficient of heavy water in normal water is very small and flow within vessels is laminar, other processes might still contribute to generating diffusion along the xylem. For example, as the water moves through the complex network of vessels, differences in velocities between vessels of different sizes cause some particles to move faster or slower than average flow. According to the Hagen–Poiseuille law, the flow in each vessel is proportional to the fourth power of the vessel radius and the mean velocity to the square of the radius, thus potentially generating large differences in particle velocities depending on the vessel size distribution and other anatomical properties. Even within a single vessel, velocity is parabolic with a maximum flow velocity in the center and zero at the vessel walls.

4.4. A way forward

The observed large δ_{xyl} variance and temporal dynamics in the empirical data suggest the need for a critical assessment of the stable isotope tracer technique for RWU studies. However, it also creates new opportunities. Since δ_{xyl} variance and temporal dynamics herein likely relate to various plant physiological processes, monitoring of variation in δ_{xyl} can allow a more integrated understanding of plant water transport and hydraulic properties.

Combining a plant hydraulic model with *in situ* SF_V, $\delta^2H_{S,i}$ and $\Psi_{S,i,t}$ can also help improve the robustness of RWU assessment and interpretation. Measurements of $\delta^2H_{S,i}$ and $\Psi_{S,i,t}$ at multiple depths, i.e. by installing soil water suction cups working at a vacuum (i.e. Rennenberg *et al.*, 1996) and multiple soil matric potential sensors that measure at a high temporal frequency, should be especially valuable since the SWIFT model showed high sensitivity to alterations of this variable and these can be directly supplied as model inputs. At

626 the same time, the availability of SF_t measurements allows for identifying the moment when
627 water uptake from all root layers is at its maximum, which can be used to determine the optimal
628 timing of sampling at a given height providing a more robust estimation of average RWU depth
629 and uptake.

630 Alongside the modeling approach presented here, new ways to study δ^2H_X at a high
631 temporal scale are strongly encouraged. For example, the pioneering work of Volkmann *et al.*
632 (2016) to the development of an *in situ* continuous isotope measurement technique that offers
633 the possibility for monitoring δ_{xyl} at a sub-hourly resolution. This technique holds strong
634 promise for further elucidating the natural δ^2H_X variances found within plants and the
635 physiology processes from which these variances result. Such high temporal resolution of
636 isotope measurements, coupled with *in situ* monitoring of various environmental and plant
637 biophysical metrics, are needed for both model improvement and further validation. Moreover,
638 these seem inevitable to eventually differentiate all causal mechanisms of the observed intra-
639 individual δ_{xyl} variance.

640

641 ## 5. Conclusions

642 A collection of empirical field data show pronounced variance and high temporal
643 fluctuations in δ_{xyl}. Moreover, these high temporal fluctuations in δ_{xyl} emanate from basic plant
644 hydraulic functioning as model explorations show. We expect the observed δ_{xyl} variance and
645 sub-daily fluctuations result, for a large part, from the mechanisms considered here, though
646 various other physiological processes could also affect δ_{xyl}.

647 Our theoretical explorations warn that variability in the isotope composition of plant
648 xylem water can result in erroneous average RWU depth estimation and will complicate the
649 interpretation and comparison of data: samples taken at different heights, times or plants

differing in SF_V may incorrectly show differences in average RWU depth. We further predict that various soil parameters and plant hydraulic parameters affect (i) the absolute size of the error and (ii) the probability of measuring δ_{xyl} values that do not represent the well-mixed values during the plants' peak RWU. Hydraulic models, such as SWIFT, could help to design more robust sampling regimes that enable improved comparisons between studied plants. We advocate the addition of SF_t, which indirectly reflects diurnal RWU fluctuations, and $\Psi_{S,i,t}$ monitoring as a minimum in future RWU assessments since these parameters were predicted to be the predominant factors introducing variance in δ_{xyl} from the SWIFT model exploration. However, soil texture and root permeability are also key measurements especially when comparing across species and sites.

Our findings do not exclude additional factors that impact the observed intra-individual δ_{xyl} variance and temporal fluctuation as many processes can act simultaneously and are not mutually exclusive. Therefore, we strongly emphasize the need for more research. Directed studies that validate and quantify the relative impact of other plant physiological processes towards variance in δ_{xyl} are a prerequisite before improved modeling tools can be developed.

Acknowledgment

This research was funded by the European Research Council Starting Grant 637643 (TREECLIMBERS), the FWO grants (1507818N, V401018N to HDD), the Carbon Mitigation Initiative at Princeton University (MD, MDV), Agence Nationale de la Recherche "Investissement d'Avenir" grant (CEBA: ANR-10-LABX-25-01), the Belgian American Educational Foundation (BAEF to FM) and the WBI (FM). LW acknowledges partial support from the Division of Earth Sciences of National Science Foundation (EAR-1554894). We are grateful to Samuel Bodé, Megan Bartlett, Isabel Martinez Cano, and Pedro Hervé-Fernández

who provided feedback on analytical and interpretative aspects of the study. We thank Dries Van Der Heyden, Wim Van Nunen, Laurence Stalmans, Oscar Vercleyen, Katja Van Nieuland, Stijn Vandevoorde, and Clément Stahl for data collection and lab processing. We credit Pascal Petronelli and Bruce Hoffman for species identification, and Cora N. Betsinger for proofreading. Cheng-Wei Huang's work provided inspiration for this research.

Author contribution

H.V., M.D.V, and P.B. supervised and provided guidance throughout all aspects of the research. H.D.D., M.D.V, and H.V. designed the study. H.D.D., K.K., R.K.M., J.D.M., L.W., and L.Z. collected and processed the empirical datasets. The model was developed and coded by H.D.D, M.D.V, M.D., and F.M. All authors contributed to the interpretation of the results and the text of the manuscript.

Data availability

Both the French Guiana data and the SWIFT model are available on the GitHub repository HannesDeDeurwaerder/SWIFT. For the availability of the data collected in China and Germany, readers are referred to Zhao *et al.* (2014) and Magh *et al.* (2020), respectively.

Competing interests

The authors declare that they have no conflict of interest.

References

Araguás-Araguás L, Froehlich K, Rozanski K. **1998**. Stable isotope composition of precipitation over southeast Asia. *Journal of Geophysical Research: Atmospheres* **103**: 28721–28742.

Azzalini A. **2013**. *The skew-normal and related families*. Cambridge University Press.

Barbeta A, Gimeno TE, Clavé L, Fréjaville B, Jones SP, Delvigne C, Wingate L, Ogée J. **2020**. An explanation for the isotopic offset between soil and stem water in a temperate tree species. *New Phytologist*.

Barnard RL, De Bello F, Gilgen AK, Buchmann N. **2006**. The δ18O of root crown water best reflects source water δ18O in different types of herbaceous species, Rapid Commun. Mass Sp., 20, 3799–3802.

Brinkmann N, Eugster W, Buchmann N, Kahmen A. **2019**. Species-specific differences in water uptake depth of mature temperate trees vary with water availability in the soil. *Plant Biology* **21**: 71–81.

Čermák J, Ulrich R, Staněk Z, Koller J, Aubrecht L. **2006**. Electrical measurement of tree root absorbing surfaces by the earth impedance method: 2. Verification based on allometric relationships and root severing experiments. *Tree physiology* **26**: 1113–1121.

Cernusak LA, Farquhar GD, Pate JS. **2005**. Environmental and physiological controls over oxygen and carbon isotope composition of Tasmanian blue gum, Eucalyptus globulus. *Tree physiology* **25**: 129–146.

Chen Y, Cao K, Schnitzer SA, Fan Z, Zhang J, Bongers F, Chen Y. **2015**. Water-use advantage for lianas over trees in tropical seasonal forests. : 128–136.

Clapp RB, Hornberger GM. **1978**. Empirical equations for some soil hydraulic properties. *Water resources research* **14**: 601–604.

Cooper LW, DeNiro MJ, Keeley JE. **1991**. The relationship between stable oxygen and hydrogen isotope ratios of water in astomatal plants.

Dawson TE, Ehleringer JR. **1991**. Streamside trees that do not use stream water. *Nature* **350**: 335–337.

Dawson TE, Ehleringer JR. **1993**. Isotopic enrichment of water in the "woody" tissues of plants: implications for plant water source, water uptake, and other studies which use the stable isotopic composition of cellulose. *Geochimica et Cosmochimica Acta* **57**: 3487–3492.

Dawson TE, Mambelli S, Plamboeck AH, Templer PH, Tu KP. **2002**. Stable isotopes in plant ecology. *Annual review of ecology and systematics* **33**: 507–559.

De Deurwaerder H, Hervé-Fernández P, Stahl C, Burban B, Petronelli P, Hoffman B, Bonal D, Boeckx P, Verbeeck H. **2018**. Liana and tree below-ground water competition—evidence for water resource partitioning during the dry season. *Tree Physiology*.

Doussan C, Pierret A, Garrigues E, Pagès L. **2006**. Water uptake by plant roots: II–modelling of water transfer in the soil root-system with explicit account of flow within the root system–comparison with experiments. *Plant and soil* **283**: 99–117.

Ehleringer JR, Dawson TE. **1992**. Water uptake by plants: perspectives from stable isotope

composition. *Plant, Cell & Environment* **15**: 1073–1082.

Ellsworth PZ, Williams DG. **2007**. Hydrogen isotope fractionation during water uptake by woody xerophytes. *Plant and Soil* **291**: 93–107.

Epila J, Maes WH, Verbeeck H, Camp J Van, Okullo JBL, Steppe K. **2017**. Plant measurements on African tropical Maesopsis eminii seedlings contradict pioneering water use behaviour. *Environmental and Experimental Botany* **135**: 27–37.

Früh T, Kurth W. **1999**. The hydraulic system of trees: theoretical framework and numerical simulation. *Journal of theoretical Biology* **201**: 251–270.

Gessler A, Brandes E, Keitel C, Boda S, Kayler ZE, Granier A, Barbour M, Farquhar GD, Treydte K. **2013**. The oxygen isotope enrichment of leaf-exported assimilates–does it always reflect lamina leaf water enrichment? *New Phytologist* **200**: 144–157.

Goldsmith GR, Muñoz-Villers LE, Holwerda F, McDonnell JJ, Asbjornsen H, Dawson TE. **2012**. Stable isotopes reveal linkages among ecohydrological processes in a seasonally dry tropical montane cloud forest. *Ecohydrology* **5**: 779–790.

Goldstein G, Andrade JL, Meinzer FC, Holbrook NM, Cavelier J, Jackson P, Celis A. **1998**. Stem water storage and diurnal patterns of water use in tropical forest canopy trees. *Plant, Cell & Environment* **21**: 397–406.

Hervé-Fernández P, Oyarzún C, Brumbt C, Huygens D, Bodé S, Verhoest NEC, Boeckx P. **2016**. Assessing the 'two water worlds' hypothesis and water sources for native and exotic evergreen species in south-central Chile. *Hydrological Processes* **30**: 4227–4241.

Huang C, Domec J, Ward EJ, Duman T, Manoli G, Parolari AJ, Katul GG. **2017**. The effect of plant water storage on water fluxes within the coupled soil–plant system. *New Phytologist* **213**: 1093–1106.

Jackson PC, Cavelier J, Goldstein G, Meunzer FC, Holbrook NM. **1995**. Partitioning of water-resources among plants of a lowland tropical forest. *Oecologia* **101**: 197–203.

De Jong van Lier Q, Van Dam JC, Metselaar K, De Jong R, Duijnisveld WHM. **2008**. Macroscopic root water uptake distribution using a matric flux potential approach. *Vadose Zone Journal* **7**: 1065–1078.

Knipfer T, Cuneo I, Brodersen C, McElrone AJ. **2016**. In-situ visualization of the dynamics in xylem embolism formation and removal in the absence of root pressure: a study on excised grapevine stems. *Plant Physiology*: pp-00136.

Lanning M, Wang L, Benson M, Zhang Q, Novick KA. **2020**. Canopy isotopic investigation reveals different water uptake dynamics of maples and oaks. *Phytochemistry* **175**: 112389.

Lin G, Sternberg L. **1993**. Hydrogen isotopic fractionation by plant roots during water uptake in coastal wetland plants. Stable isotopes and plant carbon-water relations. Elsevier, 497–510.

Magh R-K, Eiferle C, Burzlaff T, Dannenmann M, Rennenberg H, Dubbert M. **2020**. Competition for water rather than facilitation in mixed beech-fir forests after drying-wetting cycle. *Journal of Hydrology*: 124944.

Mamonov AB, Coalson RD, Zeidel ML, Mathai JC. **2007**. Water and deuterium oxide

permeability through aquaporin 1: MD predictions and experimental verification. *The Journal of general physiology* **130**: 111–116.

Marshall JD, Cuntz M, Beyer M, Dubbert M, Kuehnhammer K. **2020**. Borehole equilibration: testing a new method to monitor the isotopic composition of tree xylem water in situ. *Frontiers in Plant Science* **11**: 358.

Meinzer FC, Andrade JL, Goldstein G, Holbrook NM, Cavelier J, Wright SJ. **1999**. Partitioning of soil water among canopy trees in a seasonally dry tropical forest. *Oecologia* **121**: 293–301.

Meißner M, Köhler M, Schwendenmann L, Hölscher D. **2012**. Partitioning of soil water among canopy trees during a soil desiccation period in a temperate mixed forest. *Biogeosciences* **9**: 3465–3474.

Meng W, Xia Y, Chen Y, Pu X. **2018**. Measuring the mutual diffusion coefficient of heavy water in normal water using a double liquid-core cylindrical lens. *Scientific reports* **8**: 1–7.

Meunier F, Rothfuss Y, Bariac T, Biron P, Richard P, Durand J-L, Couvreur V, Vanderborght J, Javaux M. **2017**. Measuring and modeling hydraulic lift of Lolium multiflorum using stable water isotopes. *Vadose Zone Journal*.

Morris H, Plavcová L, Cvecko P, Fichtler E, Gillingham MAF, Martínez-Cabrera HI, McGlinn DJ, Wheeler E, Zheng J, Ziemińska K. **2016**. A global analysis of parenchyma tissue fractions in secondary xylem of seed plants. *New Phytologist* **209**: 1553–1565.

Muñoz-Villers LE, Geris J, Alvarado-Barrientos S, Holwerda F, Dawson TE. **2019**. Coffee and shade trees show complementary use of soil water in a traditional agroforestry ecosystem. *Hydrology and Earth System Sciences Discussion*.

Orlowski N, Frede HG, Brüggemann N, Breuer L. **2013**. Validation and application of a cryogenic vacuum extraction system for soil and plant water extraction for isotope analysis. *J. Sens. Sens. Syst* **2**: 179–193.

Penna D, Hopp L, Scandellari F, Allen ST, Benettin P, Beyer M, Geris J, Klaus J, Marshall JD, Schwendenmann L. **2018**. Ideas and perspectives: Tracing terrestrial ecosystem water fluxes using hydrogen and oxygen stable isotopes–challenges and opportunities from an interdisciplinary perspective. *Biogeosciences*.

Phillips DL, Gregg JW. **2003**. Source partitioning using stable isotopes: coping with too many sources. *Oecologia* **136**: 261–269.

Rennenberg H, Schneider S, Weber P. **1996**. Analysis of uptake and allocation of nitrogen and sulphur compounds by trees in the field. *Journal of Experimental Botany* **47**: 1491–1498.

Rothfuss Y, Javaux M. **2017**. Reviews and syntheses: Isotopic approaches to quantify root water uptake: a review and comparison of methods. *Biogeosciences* **14**: 2199.

Salleo S, Trifilò P, Esposito S, Nardini A, Gullo MA Lo. **2009**. Starch-to-sugar conversion in wood parenchyma of field-growing Laurus nobilis plants: a component of the signal pathway for embolism repair? *Functional Plant Biology* **36**: 815–825.

Scholander PF. **1966**. The role of solvent pressure in osmotic systems. *Proceedings of the National Academy of Sciences of the United States of America* **55**: 1407.

Secchi F, Pagliarani C, Zwieniecki MA. **2017**. The functional role of xylem parenchyma cells and aquaporins during recovery from severe water stress. *Plant, cell & environment* **40**:

858–871.

Steppe K, Lemeur R. **2004**. An experimental system for analysis of the dynamic sap-flow characteristics in young trees: results of a beech tree. *Functional Plant Biology* **31**: 83–92.

Steppe K, De Pauw DJW, Doody TM, Teskey RO. **2010**. A comparison of sap flux density using thermal dissipation, heat pulse velocity and heat field deformation methods. *Agricultural and Forest Meteorology* **150**: 1046–1056.

Vargas AI, Schaffer B, Yuhong L, Sternberg L da SL. **2017**. Testing plant use of mobile vs immobile soil water sources using stable isotope experiments. *New Phytologist* **215**: 582–594.

Vogel T, Dohnal M, Dusek J, Votrubova J, Tesar M. **2013**. Macroscopic modeling of plant water uptake in a forest stand involving root-mediated soil water redistribution. *Vadose Zone Journal* **12**.

Volkmann THM, Kühnhammer K, Herbstritt B, Gessler A, Weiler M. **2016**. A method for in situ monitoring of the isotope composition of tree xylem water using laser spectroscopy. *Plant, cell & environment* **39**: 2055–2063.

Walker CD, Richardson SB. **1991**. The use of stable isotopes of water in characterizing the source of water in vegetation. *Chemical Geology* **94**: 145–158.

Wershaw RL, Friedman I, Heller SJ, Frank PA. **1966**. Hydrogen isotopic fractionation of water passing through trees. *Advances in organic geochemistry*: 55.

White JWC, Cook ER, Lawrence JR, Broecker WS. **1985**. The D/H ratios of sap in trees - implications for water sources and tree-ring D/H ratios. *Geochimica et Cosmochimica Acta* **49**: 237–246.

De Wispelaere L, Bodé S, Hervé-Fernández P, Hemp A, Verschuren D, Boeckx P. **2016**. Plant water resource partitioning and xylem-leaf deuterium enrichment in a seasonally dry tropical climate. *Biogeosciences Discuss.* **2016**: 1–26.

Yakir D. **1992**. Variations in the natural abundance of oxygen-18 and deuterium in plant carbohydrates. *Plant, Cell & Environment* **15**: 1005–1020.

Yang Q, Xiao H, Zhao L, Zhou M, Li C, Cao S. **2010**. Stable isotope techniques in plant water sources: a review. *Sciences in Cold and Arid Regions* **2**: 112–122.

Zhao L, Wang L, Cernusak LA, Liu X, Xiao H, Zhou M, Zhang S. **2016**. Significant difference in hydrogen isotope composition between xylem and tissue water in Populus euphratica. *Plant, Cell & Environment* **39**: 1848–1857.

Zhao L, Wang L, Liu X, Xiao H, Ruan Y, Zhou M. **2014**. The patterns and implications of diurnal variations in the d-excess of plant water, shallow soil water and air moisture. *Hydrol. Earth Syst. Sci.* **18**: 4129–4151.

Zhao L, Xiao H, Zhou J, Wang L, Cheng G, Zhou M, Yin L, McCabe MF. **2011**. Detailed assessment of isotope ratio infrared spectroscopy and isotope ratio mass spectrometry for the stable isotope analysis of plant and soil waters. *Rapid Communications in Mass Spectrometry* **25**: 3071–3082.

Zimmermann U, Ehhalt D, Münnich K. **1967**. Soil-Water movement and evapotranspiration: changes in the isotopic composition of the water. Conference on Isotopes in Hydrology. Vienna, 567-585.

Tables

Table 1. Nomenclature.

Symbol	Description	Unit
$A_{R,i}$	The absorptive root area distribution over soil layer i	m^2
A_{Rtot}	The plants' total active fine root surface area	m^2
$A_{SAPWOOD}$	Sapwood area	m^2
A_x	Total lumen area	m^2
b	Shape parameter for the soil hydraulic properties (Clapp & Hornberger, 1978)	dimensionless
B_i	The overall root length density distribution per unit of soil, not necessarily limited to the focal plant.	$m\ m^{-3}$
$\delta^2 H_{X,0,t}$	Isotope composition of plant xylem water at stem base at time *t*	in ‰ VSMOW
$\delta^2 H_{X,h,t}$	Isotope composition of plant xylem water at height *h* and time *t*	in ‰ VSMOW
$\delta^2 H_{S,i}$	Isotope composition of soil water of the i^{th} soil layer (constant over time)	in ‰ VSMOW
δ_{sample}	Isotope composition of water within a sample	in ‰ VSMOW
$\Delta\widehat{\Psi}_{i,t}$	Estimated water potential gradient between stem base and the i^{th} soil layer at time *t* derived from Eq. (8)	m
$\Delta\Psi_{i,t}$	Soil matric potential gradient between soil and roots at the i^{th} soil layer at time *t*	m H_2O
$\beta^2 H_X$; $\beta^{18} O_X$	Normalized isotope composition of plant xylem water	in ‰ VSMOW
$f_{i,t}$	The fraction of water taken up in the i^{th} soil layer at time *t*	dimensionless
h	Measurement height	m
i	Soil layer index	dimensionless
δ_{xyl}	Isotope composition of plant xylem water	in ‰ VSMOW
k_i	Soil-root conductance of the i^{th} soil layer	s^{-1}
K_{max}	Maximum soil hydraulic conductivity	$m\ s^{-1}$
k_R	Effective root radial conductivity	s^{-1}
k_S	The conductance associated with the radial water flow between the soil and the root surface	s^{-1}
$K_{S,i}$	Soil hydraulic conductivity at the i^{th} soil layer	$m\ s^{-1}$
ℓ	The approximated radial pathway length of water flow between bulk soil and root surface	m
LF	Lumen fraction per unit sapwood area	$m^2\ m^{-2}$
n	Number of unique contributing water sources	#
Ψ_{sat}	Soil matric potential at soil saturation	m
$\Psi_{S,i,t}$	Soil matric potential of the i^{th} soil layer at time *t*	m
$\Psi_{X,0,t}$	Water potential at the base of the plant stem at time *t*	m
R	Heavy to light isotope ratio measured in the sample or standard	%

$RWU_{i,t}$	Net amount of water entering and leaving the root tissues per unit of time in the i^{th} soil layer at time t	$m^3\ s^{-1}$
SF_t	Instantaneous sap flow at time t	$m^3\ s^{-1}$
SF_S	Sap flow velocity, calculated as the sap flow per sapwood area	$m\ h^{-1}$
SF_V	True sap flux density, calculated as the sap flow per lumen area	$m\ h^{-1}$
τ	Delay before the isotope composition of xylem water at stem base reaches stem height h	s
θ_{sat}	Soil moisture content at soil saturation	$m^3\ m^{-3}$
$\theta_{S,i,t}$	Soil moisture content of the i^{th} soil layer at time t	$m^3\ m^{-3}$
z_i	Soil depth of the i^{th} soil layer	m

863

864

Figures

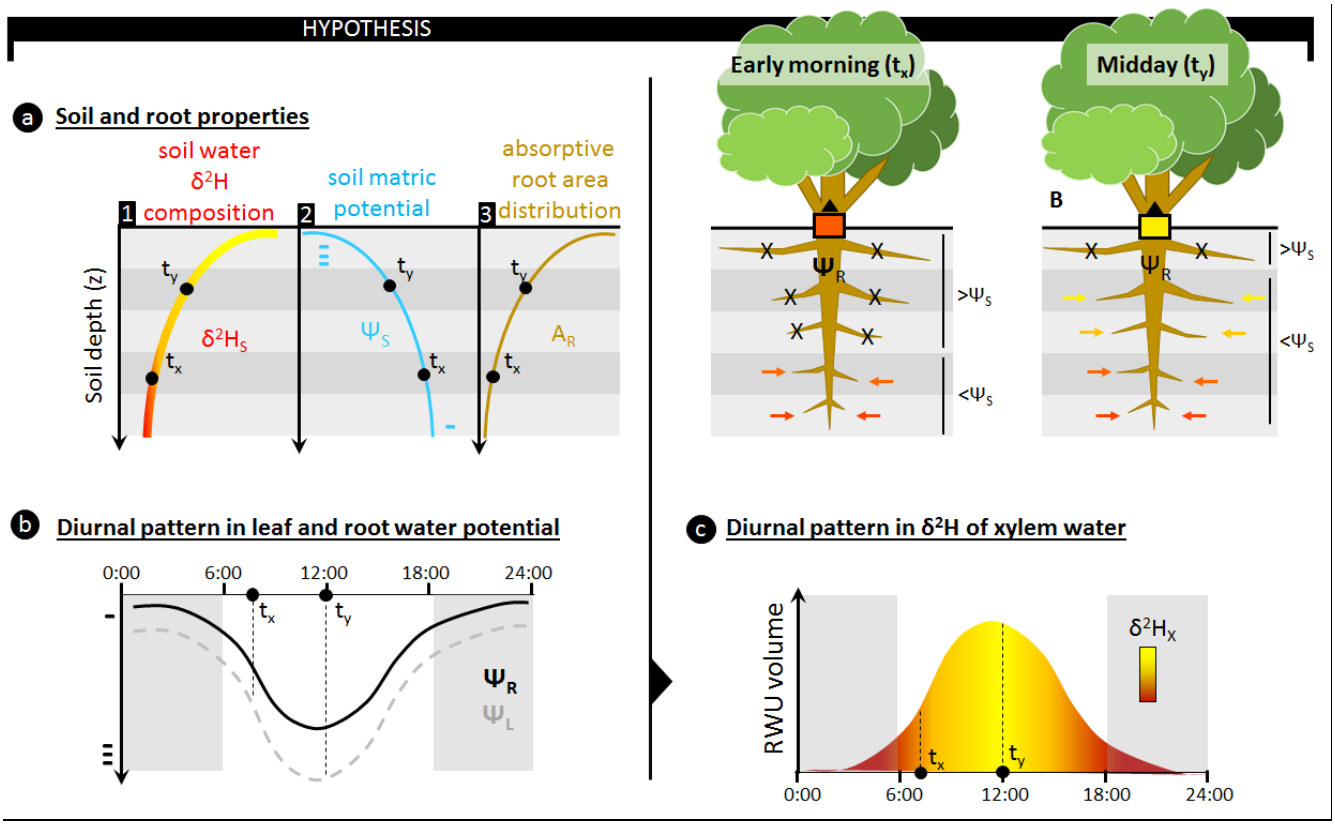

Fig 1. The use of stable water isotopes (δ^2H and $\delta^{18}O$) to assess the relative depth of root water uptake (RWU) requires a depth gradient in isotopic composition of soil water (δ^2H_S) to be present (**a, line 1**), as only then can the relative contribution of different soil layers to the isotopic composition in a plant's xylem water (δ^2H_X) be derived. These δ^2H_S gradients occur naturally as the result of evaporative soil drying during drought conditions, however, these conditions also result in the formation of a gradient in soil matric potential (Ψ_S), ensuring an increasing Ψ_S with depth (**a, line 2**). RWU and sap flow in plants are passive processes where water flows in the direction of decreasing water potentials. Specifically for RWU, this implies that water influx through the absorptive root area (A_R; **a, line 3**) of a plant's root is facilitated whenever the water potential in the root (Ψ_R) is more negative than the surrounding Ψ_S. As A_R and Ψ_S are generally not uniform with soil depth (z), the relative contribution of a specific soil layer to RWU will depend on (i) the difference between Ψ_S and Ψ_R in that soil layer, and (ii) the relative amount of absorptive root area in that soil layer. Stable water isotopes techniques

assume that the δ^2H_X reflects the contribution of δ^2H_S from all soil layers. However, this does not account for diurnal fluctuations in Ψ_R which are invoked by the diurnal patterns in a plant's transpiratory water demands (**panel b**). Typically, more negative Ψ_R values are observed when water demands are high, i.e. around midday. However, a decrease in Ψ_R will result in higher RWU, and alter the contribution of different soil layers to RWU. Specifically, dryer and shallower soil layers, with more negative Ψ_S, could start contributing to RWU as Ψ_R decreases (**panel c**). For example, in the early morning (situation t_x) when Ψ_R is high, only deeper soil layers where $\Psi_S > \Psi_R$ contribute to overall δ^2H composition of the RWU flux. As Ψ_L and Ψ_R decrease towards midday (situation t_y) more water can be absorbed from shallower soil layers. As the A_R in these shallow soil layers is high, they strongly affect the relative contribution of δ^2H_S entering the plant. Hence, diurnal fluctuations in Ψ_R will result in fluctuating mixtures of δ^2H_S entering the plant. As these δ^2H_S mixtures are transported along the xylem pathway, they produce variance in δ^2H_X, which could complicate RWU assessments via stable water isotope analysis.

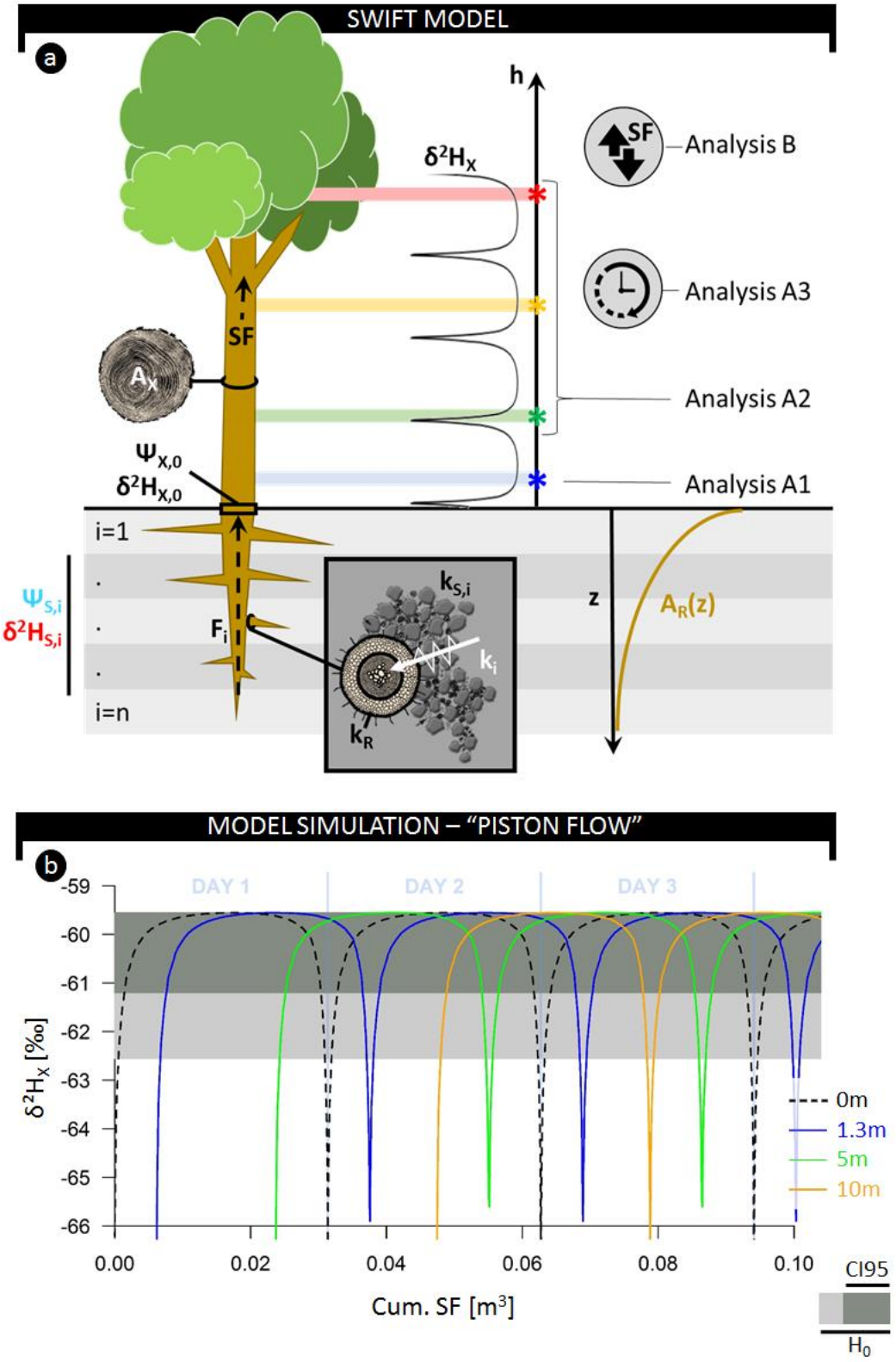
SWIFT MODEL
a
h
δ^2H_X
SF
Analysis B
Analysis A3
Analysis A2
Analysis A1
A_X
$\Psi_{X,0}$
$\delta^2H_{X,0}$
i=1
$\Psi_{S,i}$
$\delta^2H_{S,i}$
F_i
$k_{S,i}$
k_i
k_R
z
$A_R(z)$
i=n
MODEL SIMULATION – "PISTON FLOW"
b
DAY 1
DAY 2
DAY 3
δ^2H_X [‰]
-59
-60
-61
-62
-63
-64
-65
-66
0.00
0.02
0.04
0.06
0.08
0.10
Cum. SF [m³]
0m
1.3m
5m
10m
CI95
H_0

Fig. 2. (a) Schematic representation of the model and considered analysis detailed in the text. **(b)** Simulated fluctuations in δ^2H composition of plant xylem water as a function of the cumulative sap flow volume measured at various heights: stem base (0 m, black dashed), 1.3 m (blue), 5 m (green) and 10 m (red). The horizontal grey colored envelope delineates the acceptable variance from the stem mean according to the null model (H_0), i.e. assuming no variance along the length of a lignified plant aside from potential extraction error (i.e. 3‰). Herein, the dark grey envelope indicates the confidence interval comprising 95% of potential extraction error (CI95).

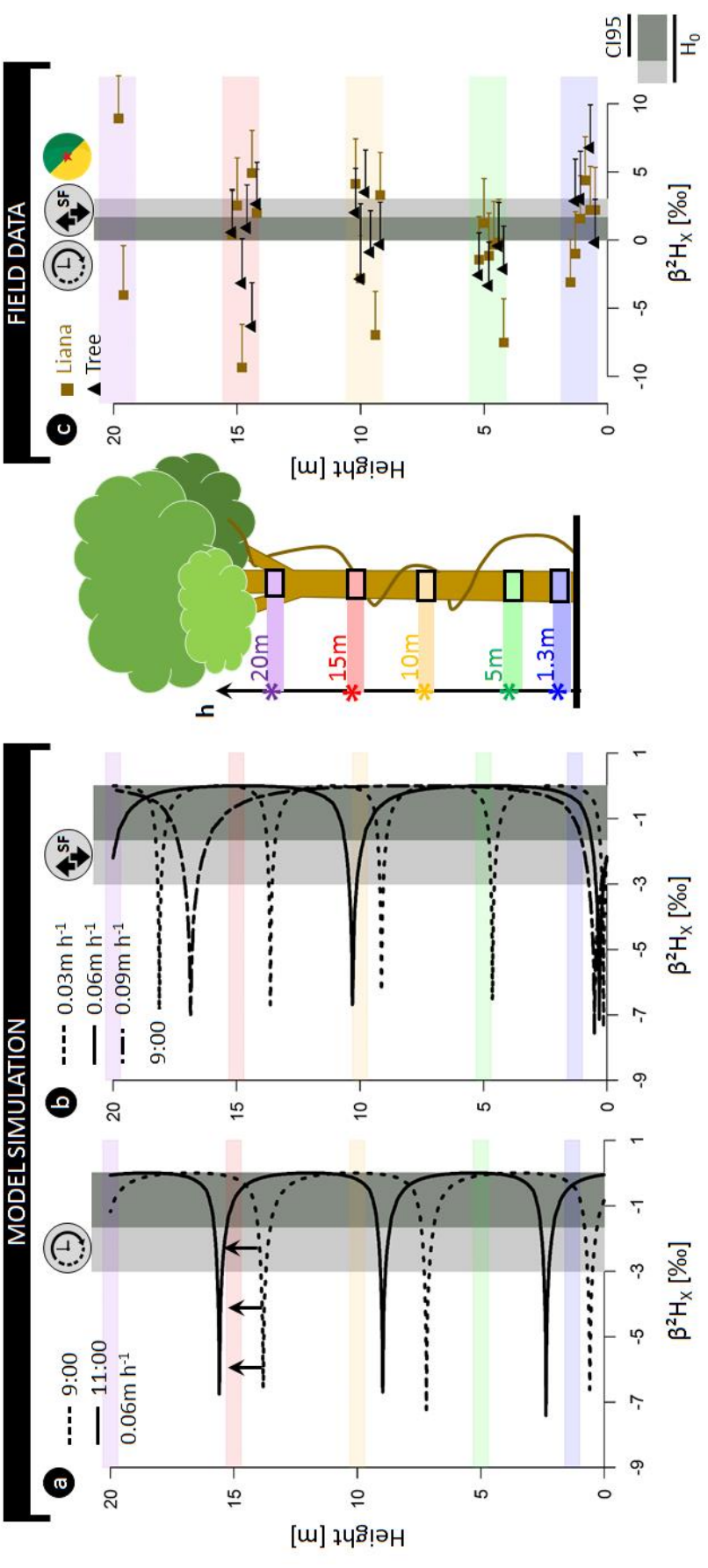
MODEL SIMULATION
FIELD DATA
a
b
c
9:00
11:00
0.06m h-1
0.03m h-1
0.06m h-1
0.09m h-1
9:00
Liana
Tree
SF
Height [m]
β2HX [‰]
CI95
H0
h
20m
15m
10m
5m
1.3m

Fig 3. (a) Model outputs for model analysis A3 representing the normalized δ^2H composition of xylem water (β^2H_X) as a function of the tree height simulated for different sampling times (9:00 and 11:00). The modeled tree has an average daily sap flux density of 0.06 m h^{-1} (SF_S; ~ daily true sap flux density SF_V = 0.42 m h^{-1}). **(b)** Model outputs for model analysis B where β^2H_X in relation to stem height is shown at 9:00 a.m., but parameterized with distinct SF_S, i.e. 0.09, 0.06 and 0.03 m h^{-1} (corresponding to SF_V of 0.64, 0.42 and 0.19 m h^{-1}, respectively). The standard parameterization used for both study analysis is detailed in Table S1. **(c)** Field measurements of β^2H_X for six lianas (■) and six trees (▲). Error whiskers are the combination of potential extraction and measurement errors of the isotope analyzer. A species-specific breakdown of the field data is provided in Fig S2. The horizontal grey colored envelope in all panels delineates the acceptable variance from the stem mean according to the null model (H_0), i.e. assuming no variance along the length of a lignified plant aside from potential extraction error (i.e. 3‰). Herein, the dark grey envelope indicates the confidence interval comprising 95% of potential extraction error (CI95).

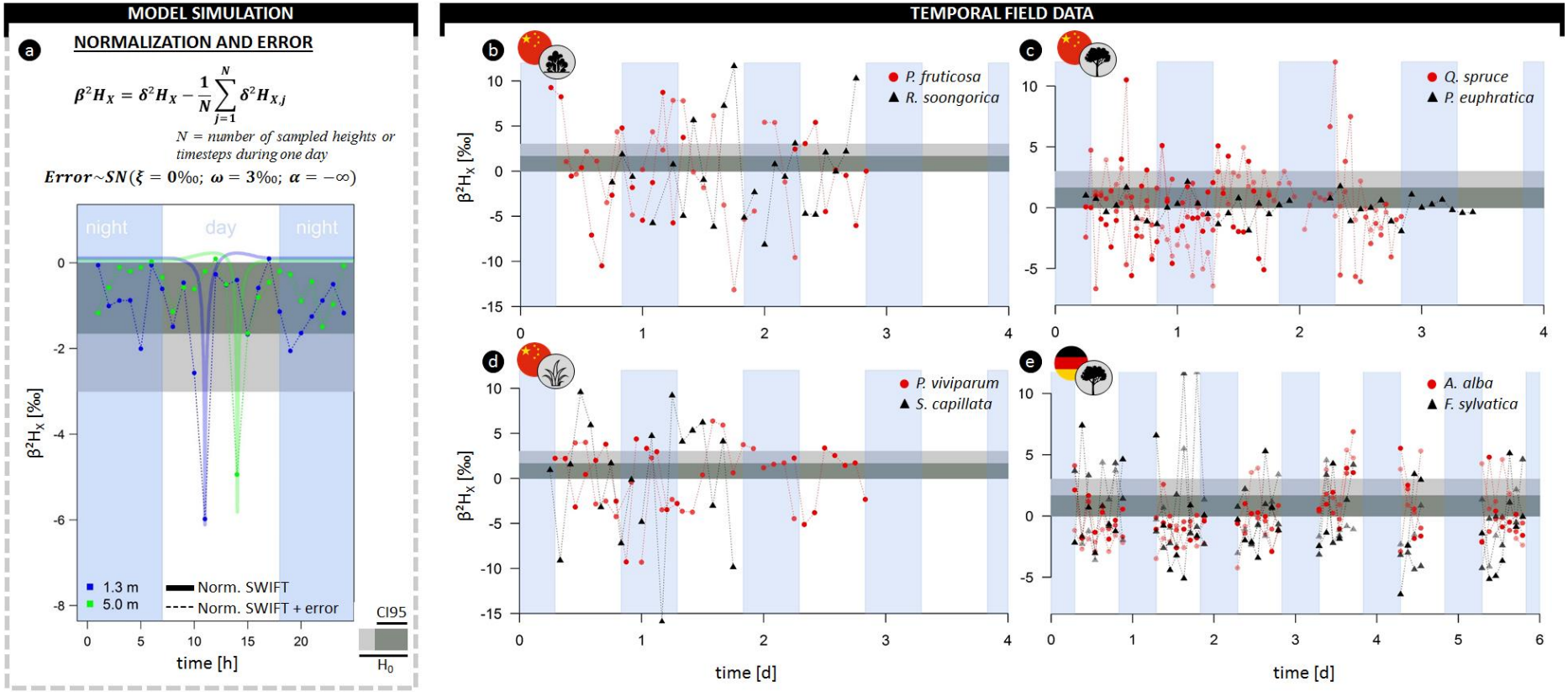
MODEL SIMULATION
a
NORMALIZATION AND ERROR
$\beta^2 H_X = \delta^2 H_X - \frac{1}{N}\sum_{j=1}^{N} \delta^2 H_{X,j}$
N = number of sampled heights or timesteps during one day
$Error \sim SN(\xi = 0‰;\ \omega = 3‰;\ \alpha = -\infty)$
night
day
night
β²H_X [‰]
time [h]
1.3 m
5.0 m
Norm. SWIFT
Norm. SWIFT + error
CI95
H0
TEMPORAL FIELD DATA
b
P. fruticosa
R. soongorica
c
Q. spruce
P. euphratica
d
P. viviparum
S. capillata
e
A. alba
F. sylvatica
β²H_X [‰]
time [d]

Fig 4. (a) Illustrative example of model simulations transformed in normalized δ^2H composition of xylem water (β^2H_X) at 1.3 (blue) and 5m (green) sampling height, with the formula provided. Thicker lines indicate model simulations without error, line connected dots indicate a scenario of hourly sampling with consideration of extraction error (i.e. a negative skew-normal distribution; ξ = 0‰, the scale ω = 3‰, and shape α = -∞). **(b-e)** High temporal field measurements of β^2H_X of (b) two shrubs, (c) two trees, and (d) two herb species sampled in the Heihe River Basin (northwestern China); and (e) two tree species sampled in the "Freiamt" field site in south-west Germany. The horizontal grey colored envelope in all panels delineates the acceptable variance from the stem mean according to the null model (H_0), i.e. assuming no variance along the length of a lignified plant aside from potential extraction error (i.e. 3‰). Herein, the dark grey envelope indicates the confidence interval comprising 95% of potential extraction error (CI95). A breakdown of the field data on species and individual level is provided in the supplementary figures (Fig S3-S4-S5-S6)

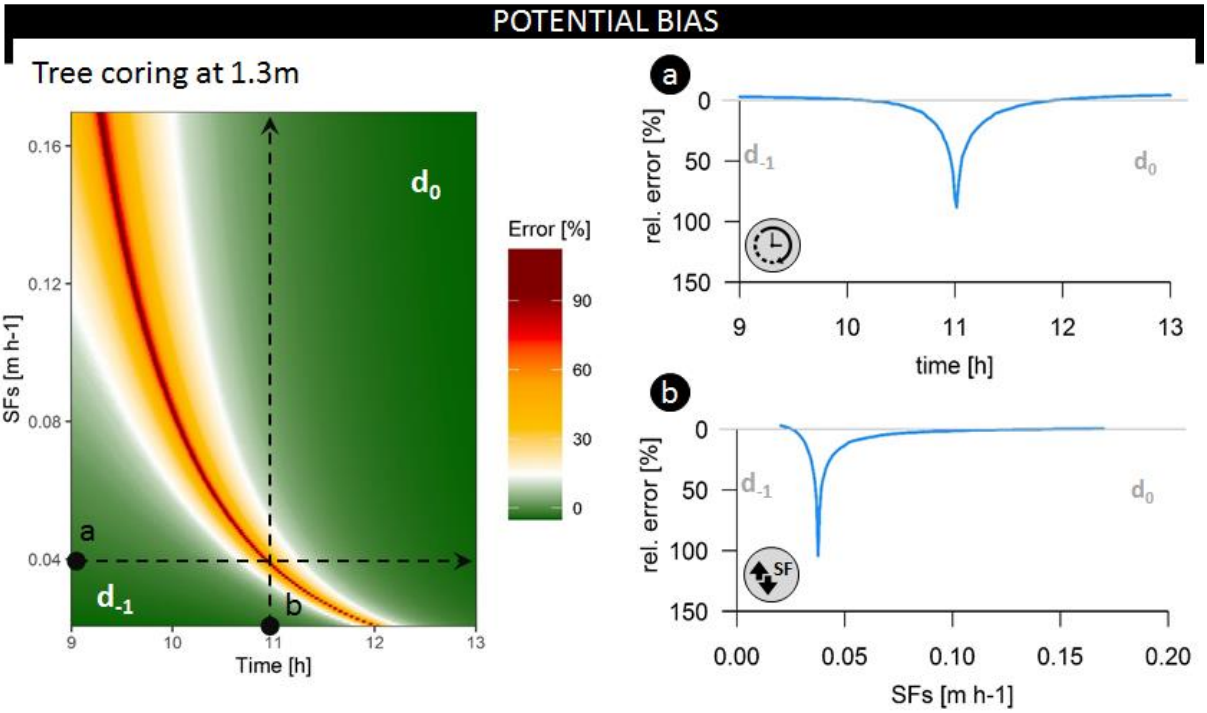

Fig 5. Relative error on the inferred average root water uptake depth (i.e. bias between the average daily and the instantaneous derived average RWU depth) at coring height of 1.3m, throughout the common sampling period (9:00 until 13:00) and over a range of potential SF_S (in m h^{-1}) – corresponding to SF_V range of 0.15–1.25 m h^{-1}. Both dotted lines describe test scenarios evaluated in the breakup panels. The dynamics in relative error when sampling **(a)** over different time steps, restricting sap flux density at 0.04 m h^{-1} (i.e. SF_V = 0.28 m h^{-1}), or **(b)** over different SF_S-values when restricting sampling time at 11 am. d_{-1} and d_0 indicate whether the derived average RWU depth error corresponds to the previous or current day of measurement.

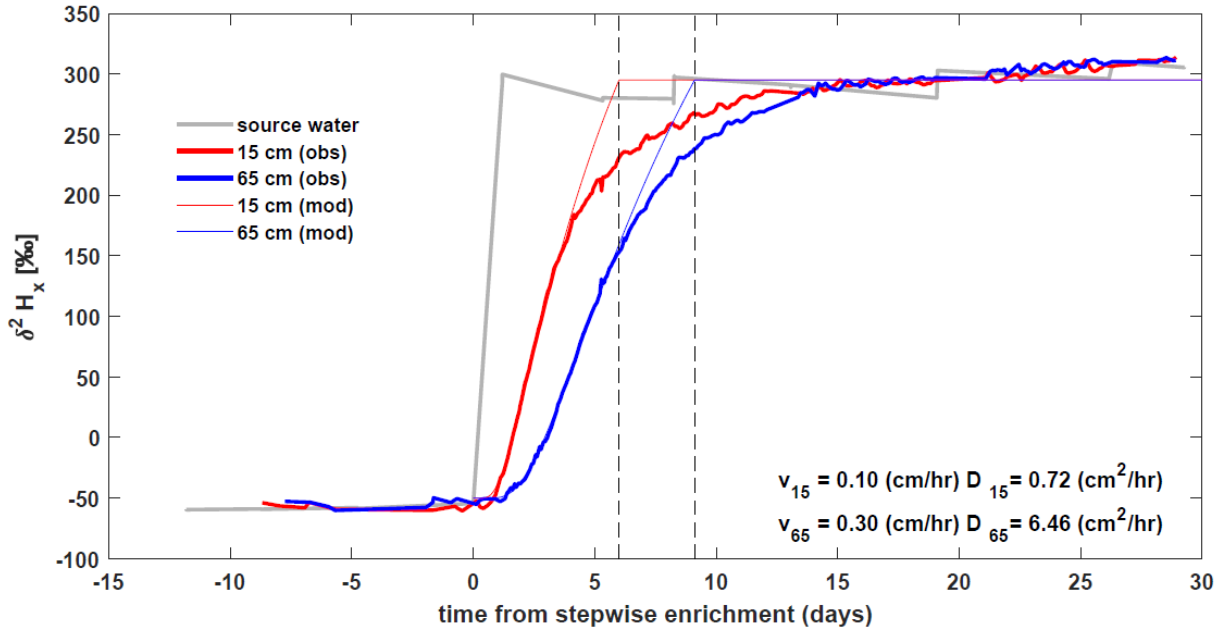

Fig. 6. Basic model validation, comparing continuous *in situ* $\delta^2 H_X$ measurements of a stepwise ^2H enrichment experiment (Marshall *et al.*, 2020) with analytical solutions of advection-diffusion equation, at heights 0.15m (—) and 0.65m (—) on a pine tree (*Pinus pinea L*). The source water of the intact-root, isotopic enrichment greenhouse experiment, is presented in grey. Model parameters, velocity, and diffusion were fitted by visual inspection independently for the two heights to match the initial increase in isotope signature (values reported in the bottom right)

Supporting Information

Article title: Causes and consequences of pronounced variation in the isotope composition of plant xylem water

Authors: Hannes P.T. De Deurwaerder, Marco D. Visser, Matteo Detto, Pascal Boeckx, Félicien Meunier, Kathrin Kuehnhammer, Ruth-Kristina Magh, John D. Marshall, Lixin Wang, Liangju Zhao, Hans Verbeeck

Method A:

Detailed description data collection French Guiana

We used data for six canopy trees and six canopy lianas sampled on two subsequent dry days (24-25 August 2017) at the Laussat Conservation Area in Northwestern French Guiana. The sampling site (05°28.604'N-053°34.250'W) lies approximately 20 km inland at an elevation of 30 m a.s.l. This lowland rainforest site has an average yearly precipitation of 2500 mm yr^{-1} (Baraloto *et al.*, 2011). Average and maximum daily temperatures of respectively 30°C and 36°C were measured during the sampling period. Sampled individuals are located in the white sands forest habitat (Baraloto *et al.*, 2011), on a white sandy ultisol with a typically high percentage of sand.

Individuals (Table A1) were selected based on the assessment of climbable tree, intactness of leafy canopy vegetation and close vicinity with one another to optimize similarity in meteorological and edaphic characteristics. Liana diameters were measured at 1.3 m from the last rooting point (Gerwing *et al.*, 2006), tree diameters were measured at 1.3 m (Table A1). Liana and tree sampling allowed highly contrasted sap flux density (Gartner *et al.*, 1990).

Sampling strategy

The stem xylem tissue of individual plants was sampled at different heights (1.3, 5, 10, 15, and 20 m where possible) at the same radial position of the stem, between 9:00 and 15:00 to assure high sap flow. Since upstream δ_{xyl} enrichment due to Péclet effect, in close vicinity to evaporative surfaces has been observed in the literature (Dawson & Ehleringer, 1993; Barnard *et al.*, 2006), sampling was restricted to coring of the main stems. The order of sampling, i.e. ascending versus descending heights, was randomized. Tree stem xylem samples were collected with an increment borer (5 mm diameter), resulting in wooden cylinders from which bark and phloem tissues were removed. Coring was performed within the horizontal plane at the predefined heights, oblique to the center of the stem to maximize xylem and minimize heartwood sampling, and slowly to avoid heating the drill head and fractionation. Taking one sample generally took between 5 and 10 minutes. Since coring lianas was not possible, we collected cross-sections of the lianas after removing the bark and phloem tissue with a knife. Soil samples were collected at different depths (0.05, 0.15, 0.30, 0.45, 0.60, 0.90, 1.20, and 1.80m) within close vicinity to the sampled individuals using a soil auger. All materials were thoroughly cleaned between sampling using a dry cloth to avoid cross-contamination. Upon collection, all samples were placed in pre-weighed glass collection vials, using tweezers, to reduce contamination of the sample. Glass vials were immediately sealed with a cap and placed in a cooling box, to avoid water loss during transportation.

Sample processing

Sample processing was performed as in De Deurwaerder *et al.* (2018). Specifically, all fresh samples were weighed, transported in a cooler, and frozen before cryogenic vacuum distillation (CVD). Water was extracted from the samples via CVD (4 h at 105°C). Water recovery rates were calculated from the fresh weight, weight after extraction, and oven-dry weight (48 h at 105°C). Samples were removed from the analysis whenever weight loss resulting from the extraction process was below 98% (after Araguás-Araguás *et al.*, 1998). Nearly all soil samples fell below this benchmark and were therefore excluded from further analysis (Fig S1). The isotope composition of the water in the samples was measured by a Wavelength-Scanned-

Cavity Ring-Down Spectrometer (WS-CRDS, L2120-i, Picarro, California, USA) coupled with a vaporizing module (A0211 High Precision Vaporizer) through a micro combustion module to avoid organic contamination (Martin-Gomez *et al.*, 2015; Evaristo *et al.*, 2016). Post-processing of raw δ-readings into calibrated δ-values was performed using SICalib (version 2.16; Gröning, 2011) and internal laboratory references, i.e. Lab1 (δ^2H: 7.74±0.4‰; δ^{18}O: 5.73±0.06‰,), Lab3 (δ^2H: -146.98±0.4‰; δ^{18}O: -20.01±0.06‰,) and quality assurance samples (δ^2H: -48.68±0.4‰; δ^{18}O: -7.36±0.06‰). Calibrated δ-values are expressed on the international V-SMOW scale.

References

Araguás‐Araguás L, Froehlich K, Rozanski K. 1998. Stable isotope composition of precipitation over southeast Asia. *Journal of Geophysical Research: Atmospheres* **103**: 28721–28742.

Baraloto C, Rabaud S, Molto Q, Blanc L, Fortunel C, Herault B, Davila N, Mesones I, Rios M, Valderrama E. 2011. Disentangling stand and environmental correlates of aboveground biomass in Amazonian forests. *Global Change Biology* **17**: 2677–2688.

Barnard RL, De Bello F, Gilgen AK, Buchmann N. 2006. The δ18O of root crown water best reflects source water δ18O in different types of herbaceous species, *Rapid Commun. Mass Sp.*, **20**, 3799–3802.

Dawson TE, Ehleringer JR. 1993. Isotopic enrichment of water in the "woody" tissues of plants: implications for plant water source, water uptake, and other studies which use the stable isotopic composition of cellulose. *Geochimica et Cosmochimica Acta* **57**: 3487–3492.

De Deurwaerder H, Hervé-Fernández P, Stahl C, Burban B, Petronelli P, Hoffman B, Bonal D, Boeckx P, Verbeeck H. 2018. Liana and tree below-ground water competition—evidence for water resource partitioning during the dry season. *Tree Physiology*. **38(7)**: 1071-1083.

Evaristo J, McDonnell JJ, Scholl MA, Bruijnzeel LA, Chun KP. 2016. Insights into plant water uptake from xylem-water isotope measurements in two tropical catchments with contrasting moisture conditions. *Hydrological Processes* **30**: 3210–3227.

Gartner BL, Bullock SH, Mooney HA, Brown VB, Whitbeck JL. 1990. Water Transport Properties of Vine and Tree Stems in a Tropical Deciduous Forest. *American Journal of Botany* **77: 742–749**.

Gerwing JJ, Schnitzer SA, Burnham RJ, Bongers F, Chave J, DeWalt SJ, Ewango CEN, Foster R, Kenfack D, Martínez‐Ramos M. 2006. A standard protocol for liana censuses. *Biotropica* **38**: 256–261.

Gröning M. 2011. Improved water δ2H and δ18O calibration and calculation of measurement uncertainty using a simple software tool. *Rapid Communications in Mass Spectrometry* **25**: 2711–2720.

Martin-Gomez P, Barbeta A, Voltas J, Penuelas J, Dennis K, Palacio S, Dawson TE, Pedro Ferrio J. 2015. Isotope-ratio infrared spectroscopy: a reliable tool for the investigation of plant-water sources? *New Phytologist* **207**: 914–927.

Table A1. Sampled liana and tree individuals, provided with their species, respective diameter at breast height (DBH, in cm) and their δ^2H and $\delta^{18}O$ ranges (in ‰, VSMOW) measured per individual.

Code	Growth form	DBH [cm]	Family	Species name	δ^2H_X-range [in ‰, VSMOW]	$\delta^{18}O_X$-range [in ‰, VSMOW]
SP1	Tree	15.6	Moraceae	*Coussapoa sp.*	-30.1; -25.5	-2.8; -2.6
SP2	Tree	50.9	Fabaceae	*Vouacapoua americana*	-23.9; -18.1	-3.1; -2.2
SP3	Tree	44.6	Vochysiaceae	*Erisma nitidum*	-27.7; -20.8	-3.2; -1.9
SP4	Tree	26.1	Sapotaceae	*Micropholis guyanensis*	-29.8; -28.0	-3.0; -2.9
SP5	Tree	21.0	Anacardiaceae	*Tapirira guyanensis*	-31.1; -18.0	-3.2; -2.2
SP6	Tree	49.7	Fabaceae	*Albizia pedicellaris*	-26.9; -22.1	-3.2; -2.6
SP1	Liana	2.8	Polygonaceae	*Coccoloba sp.*	-27.9; -20.7	-3.9; -2.3
SP2	Liana	2.7	Convolvulaceae	*sp.*	-29.3; -24.0	-4.4; -2.9
SP3	Liana	0.8	Moraceae	*sp.*	-40.8; -22.6	-4.5; -2.3
SP4	Liana	3.8	Combretaceae	*cf. rotundifolium Rich.*	-23.6; -15.2	-2.9; -2.0
SP5	Liana	0.7	Convolvulaceae	*Maripa cf violacea*	-31.6; -19.7	-3.8; -2.7
SP6	Liana	3.8	Convolvulaceae	*Maripa sp.*	-35.3; -24.4	-4.8; -3.1

Method B:

Exploring the effect of diffusion on xylem transport of isotopes

The current version of the model assumes a negligible impact of diffusion on the variance in the isotopic composition of the xylem water in the stem. Here, the validity of this assumption is discussed in more detail. We will use analytical and numerical solutions of the advection-diffusion equation to simulate the transport of isotope within the xylem, followed by a short discussion.

Theory

One-dimensional solute flux (J) of a solute concentration (C) through a pipe can be expressed as the sum of the advection and diffusion processes:

$$J = uC + q \tag{1}$$

where u is the fluid flow velocity and q the diffusion flux.

The one-directional diffusion flux along the direction *x* can be expressed by Fick's law:

$$q = -D\frac{\partial C}{\partial x} \tag{2}$$

where D ($m^2\ s^{-1}$) is the diffusion constant. The mass conservation can be written:

$$\frac{\partial C}{\partial t} = -\frac{\partial J}{\partial x} \tag{3}$$

The diffusion equation

Assuming no flow ($u = 0$) and inserting (2) into (3) we obtain:

$$\frac{\partial C}{\partial t} = D\frac{\partial^2 C}{\partial x^2} \tag{4}$$

Solutions of (4) for an instantaneous point source can be given in the form

$$C(x,t) = \frac{M}{\sqrt{4\pi Dt}} exp\left(-\frac{x^2}{4Dt}\right) \tag{5}$$

where M is the mass of solute injected uniformly across the cross-section of the pipe at $x = 0$. Using the superimposition principle, we can also derive the solution for the one-dimensional stagnant case (an initial step function concentration without advection) as

$$C(x,t) = \frac{C_0}{2} erfc\left(\frac{x}{\sqrt{4\pi Dt}}\right) \quad (6)$$

where C_0 is the initial concentration at $x < 0$ and erfc is the complementary error function.

Advection-diffusion equation

In the case of flow with velocity, (4) is modified as:

$$\frac{\partial C}{\partial t} = D\frac{\partial^2 C}{\partial x^2} + u\frac{\partial C}{\partial x} \quad (7)$$

The solution for constant concentration at $x = 0$ with initial zero concentration on a semi-infinite domain, i.e.

$$\begin{cases} C(x,0) = 0, & x > 0 \\ C(0,t) = C_0, & t > 0 \end{cases} \quad (8)$$

is given by (Ogata & Banks, 1961):

$$C(x,t) = \frac{C_0}{2}\left(erfc\left(\frac{x-ut}{\sqrt{4\pi Dt}}\right) + exp\left(\frac{xu}{D}\right) erfc\left(\frac{x+ut}{\sqrt{4\pi Dt}}\right)\right) \quad (9)$$

This solution can describe the dynamic of a solute concentration along the xylem under constant velocity, with a fixed concentration at the inlet point.

Numerical solutions

Solutions for problems with different boundary conditions and variable velocity are not available. In order to investigate the case with periodic concentrations at the inlet of the pipe and periodic velocity we used numerical solutions of the advection-diffusion equation

$$\frac{\partial C}{\partial t} = D\frac{\partial^2 C}{\partial x^2} + u_0 f(t)\frac{\partial C}{\partial x} \quad (10)$$

where $f(t)$ is a periodic function. We used the wrapped normal distribution defined as

$$f(t) = \sum_{i=-100}^{i=100} \exp\left[\frac{\left(\frac{2\pi t}{24} - \pi - 2\pi k\right)^2}{2\sigma^2}\right] \quad (11)$$

The boundary conditions at the inlet and outlet are defined as

$$\begin{cases} C = (C_{max} + C_{min})g(t) + C_{min} & x = 0, t > 0 \\ \frac{\partial C}{\partial t} = 0 & x = H, t > 0 \end{cases} \quad (12)$$

where $g(t)$ is another periodic function defined as

$$g(t) = \sum_{i=-100}^{i=100} \exp\left[\frac{\left|\frac{2\pi t}{24} - \pi - 2\pi k\right|^3}{2\sigma^3}\right] \quad (13)$$

The third power in (13) was chosen to match the diurnal cycle of the isotopic concentration at the tree base obtained by SWIFT. The equation was solved using the function *pdepe* implemented in Matlab (R2019a), explicitly designed to solve initial-boundary value problems for parabolic-elliptic partial differential equations in 1-D (Skeel & Berzins, 1990).

Unfortunately, numerical solutions of the advection-diffusion equation suffer numerical oscillation for values of the Péclet number greater than one (Zienkiewicz *et al.*, 2000), so results are presented for values of diffusivity 50, 100, 200 and 400 cm^2 hr^{-1}. These values are much larger than the diffusivity of heavy water and they will produce stronger smoothing.

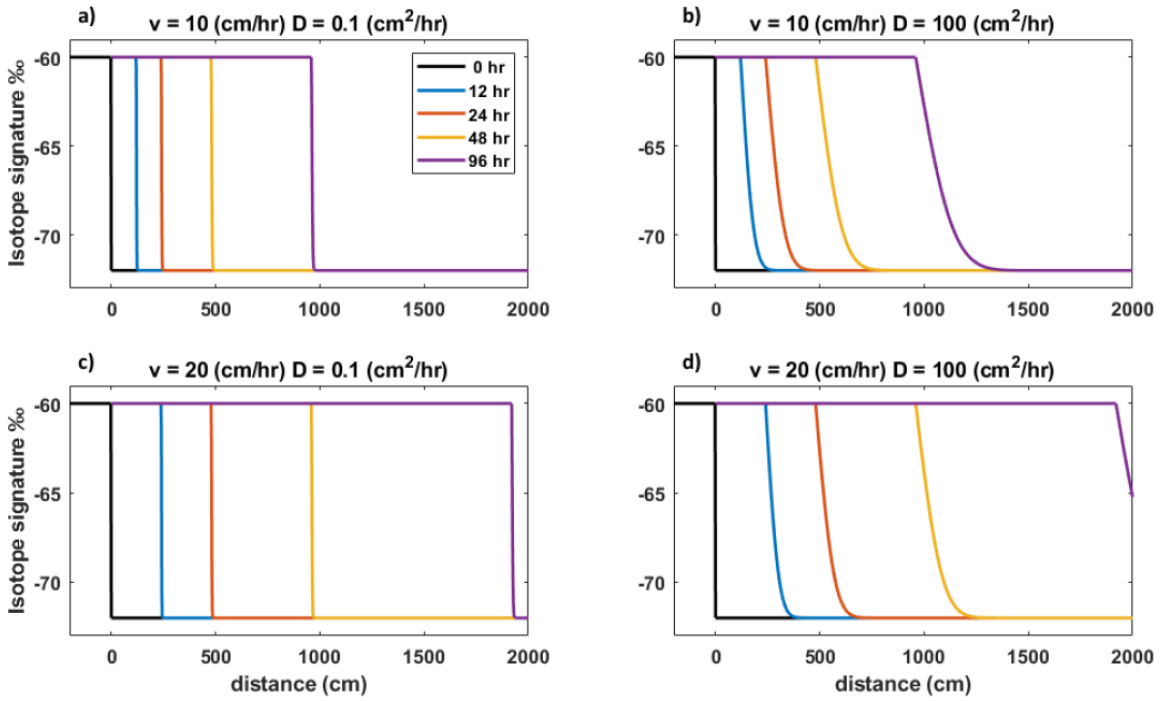

Fig B1: Analytical solutions of advection-diffusion equation on a semi-infinite 1-D domain (Eq. 9) with 12 ‰ step-change in isotope signature for different values of flow velocity and diffusivity. The plots show the impact of diffusion on the isotopic composition of xylem water. Colored lines show the solution at different time intervals: 0, 12, 24, 48, and 96 hr. Note that the values of diffusivity are much higher than these reported for heavy water (e.g. D=0.1 cm^2 h^{-1}; Meng et al., 2018)

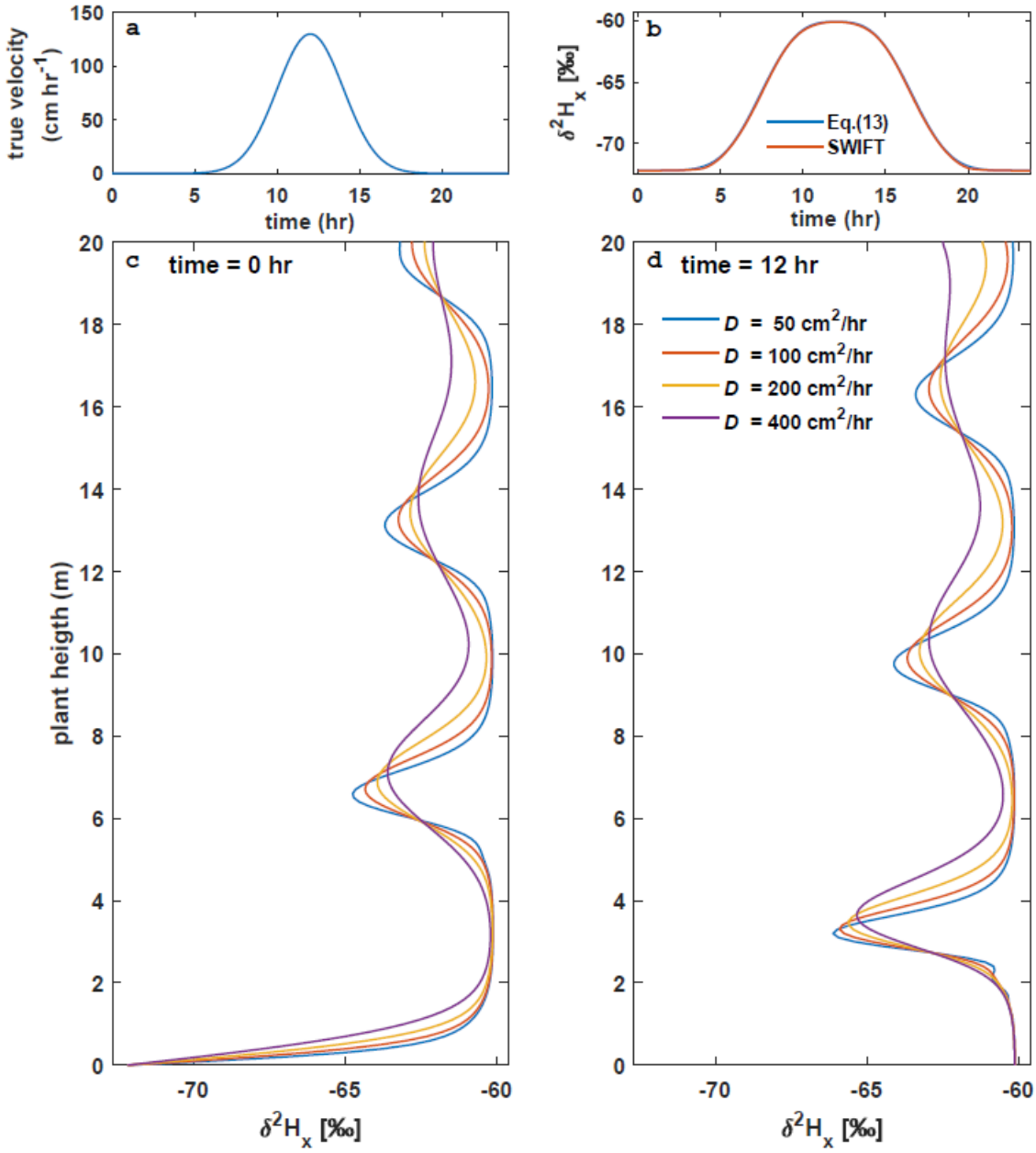

Fig B2: Numerical solutions of advection-diffusion equation on a finite 1-D domain (Eq. 10-13) with 12 ‰ step-change in isotope signature for different values of diffusivity along the length of the xylem. The periodic forcing used in the simulations are shown in panel a and b. Panels c and d show the solutions for two different time of the day. Colored lines show the solution at different diffusivity (see legend in d). Note that the values of diffusivity are much higher than these reported for heavy water (e.g. D=0.1 $cm^2\ h^{-1}$; Meng et al., 2018).

Results and Discussion

The diffusivity of ^2H in water depends on temperature: at 20 ^oC is D = 6.87 10^{-2} cm^2 hr^{-1}, at 40 ^oC is D = 1.37 10^{-1} cm^2 hr^{-1} (Meng et al., 2018). Another process that can cause substantial mixing is the random movement of particles in the xylem network. Within each vessel, the flow is laminar, but in vessels with a larger diameter, velocity is higher than in vessels with a smaller diameter. According to the Hagen–Poiseuille law, the flow is proportional to the fourth power of diameter (hence, the velocity is proportional to diameter square). Therefore, the variable velocity experienced by the particles in the xylem network can generate substantial random motion in the transport of a solute in a similar manner of diffusion in a porous media.

Molecular diffusivity results in a relatively negligible impact of diffusion on the variance in ^2H when high sap flux densities are considered, as shown in Fig B1. For example, for diffusivity of 0.1 cm^2 hr^{-1}, after 96 hours, diffusion results in smearing in a range ± 10cm (Fig. B1a). The case with a flow velocity of 25 cm hr^{-1}, comparable to the velocity of sap in xylem, shows that the transport of the solute is minimally affected by diffusion (Fig B1 a and c). In order to appreciate the effect of diffusion, the diffusivity needs to increase three orders of magnitude (Fig B1 b and d). However, because homogenization increases with time, the impact of diffusion on δ^2H dynamics can be non-negligible for very low sap flux velocities.

Numerical solutions with the periodic forcing (Fig B2 a and b), show that for high values of diffusivity there could be a substantial smoothing in the peak (Fig B2 c and d). The smoothing progress along the path-length of the flow. However, note that a very high value of diffusivity (>400 cm^2 hr^{-1}) is required for complete homogenization above 10 m.

For the general application to isotope transport in xylem with variable input concentrations and variable sap flow velocity, diffusion can cause a smoothing of the peak and a consequent increase in the width of the δ^2H_X-baseline drop. Therefore, the probability of sampling a non-representative section within this δ^2H_X-baseline might increase, which means that neglecting diffusion could lead towards a conservative assessment of the bias in RWU estimates. However, the minimal reduction of the peak in δ^2H_X over time might lead to reducing the variability in time and space compared to the case with no diffusion. In conclusion, while diffusion does affect both the absolute range of δ^2H_X variance and the width of the δ^2H_X-baseline drop (i.e. increased probability of extracting biased samples), the impact is small in the lower part of the tree and over the timeframe and sap flow flux considered in this study. Hence, for this study, diffusion will not result in the complete homogenization of the δ^2H_X along the length of the studied trees, consistent with empirical datasets (Fig 3c, Fig S2.).

References

Meng, W., Xia, Y., Chen, Y., & Pu, X. 2018. Measuring the mutual diffusion coefficient of heavy water in normal water using a double liquid-core cylindrical lens. *Scientific reports* **8(1)**: 1-7.

Ogata A, Banks RB. 1961. A solution of the differential equation of longitudinal dispersion in porous media: fluid movement in earth materials. *US Government Printing Office*.

Skeel RD, Berzins M. 1990. A method for the spatial discretization of parabolic equations in one space variable. *SIAM journal on scientific and statistical computing* **11**: 1–32.

Zienkiewicz OC, Taylor RL, Taylor RL, Taylor RL. 2000. The finite element method: solid mechanics. *Butterworth-heinemann.*

Method C:

A detailed description of the performed transport dynamics and sensitivity analyses.

Transport dynamics

The intact-root greenhouse experiment of Marshall *et al.* (2020) allows assessment if other processes besides molecular diffusivity might contribute to isotope transport through the plant, especially when very low sap flow velocities are considered. Specifically, the experiment follows the impact of a stepwise ^{2}H enrichment of the source water, i.e. from δ^2H=-59.28 ± 0.24 ‰ to δ^2H=290.57 ± 3.08‰ (see Fig 6), on the δ^2H_X dynamics in a pine tree (*Pinus pinea L.).* The tree was placed in a large pot, with the root system fully submerged in aerated water (using mini-pumps) and subjected to artificial light conditions (12h light, 12h dark, light transition at 7:00 o'clock). δ^2H_X was monitored continuously and *in situ* at two sampling heights, 0.15 cm, and 0.65 cm, respectively, using a novel borehole technique. Concomitant, sap flow velocity was measured using a sap flow sensor (heat pulse velocity sensor, Edaphic Scientific, Australia), installed at 0.85m height, and perpendicular to the upper borehole. For specific details of this experiment, we refer to Marshall *et al.* (2020).

In this setup, roots are submerged in a uniform isotopic solution, so the SWIFT model parameterization of soil and root is not necessary. The isotopic composition of the source water will, therefore, almost instantly reflect the δ^2H at the stem base. The impact of diffusion could not be considered negligible as sap flow velocities are very low (daily mean SF_V = 0.97 ± 0.39 cm h^{-1}) and the experiment lasted out 38 days before equilibrium was reached between the δ^2H_X of the source water and the δ^2H_X in both boreholes. For simulating the isotopic dynamics, we used an analytical solution of the advection-diffusion, as described in supplementary methods B, coupled to the SWIFT model. Model parameters, velocity, and diffusion were fitted by visual inspection independently for the two heights to match the initial increase in isotope signature. Note that the studied tree shows strong tapering (diam. at 0.15cm = 9.9cm; diam. at 0.65cm = 8.0cm), causing an acceleration of the sap flow along the pathway length as a same volume of water is propelled through a diminishing cross-area. This is also reflected in the allocated velocity parameters.

Sensitivity analyses

We first assessed model sensitivity to (bio)physical variables by modifying model parameters of soil type, sap flow, and root properties as compared to the standard parameterization (given in Table S1). The following sensitivity analyses were considered:

Soil type: The soil moisture content overall soil layers ($\theta_{S,i,t}$) can be deduced from the considered Meißner et al. (2012) $\Psi_{S,i,t}$ profile (see Fig. S8 and Table S1) using the Clapp & Hornberger (1978) equation:

$$\theta_{S,i,t} = \theta_{sat} \cdot \left(\frac{\Psi_{S,i,t}}{\Psi_{sat}}\right)^{-1/b} \quad \text{Eq. (1)}$$

Where θ_{sat}, Ψ_{sat} and b are soil-type specific empirical constants that correspond to sandy loam soil textures in the standard model parameterization (Clapp & Hornberger,

1978). The derived soil moisture profile ($\theta_{S,i,t}$), in turn, then provides a basis to study the impact of other soil textures. A new soil texture specific $\Psi_{S,i,t}$ profile can then be deduced by using θ_{sat}, Ψ_{sat} and b values corresponding to different soil texture types (values from Table 2 of Clapp & Hornberger (1978)). This enabled us to study $\Psi_{S,i,t}$ profiles for four distinct soil types, i.e. (i) sand, (ii) loam, (iii) sandy clay and (iv) clay soils, in relation with the original silt loam $\Psi_{S,i,t}$ profile.

Volume of water uptake: We varied the total diurnal volume of water taken up by the tree. New SF_t values are scaled using algorithms from the literature that provide an estimate of the daily sap flow volume of a tree based on its DBH (Andrade *et al.*, 2005; Cristiano *et al.*, 2015).

Root conductivity: We varied the root membrane permeability (k_R) to match multiple species-specific values found in the literature (Sands *et al.*, 1982; Rüdinger *et al.*, 1994; Steudle & Meshcheryakov, 1996; Leuschner *et al.*, 2004).

The second set of sensitivity analyses test the impact of root hydraulics, sap flux density, and sampling strategies on the sampled δ^2H_X. We obtained 1000 samples per parameter from corresponding distributions and ranges (given in Table S2) with a Latin hypercube approach (McKay *et al.*, 1979; McKay, 1988). This is a stratified sampling procedure for Monte Carlo simulation that can efficiently explore multi-dimensional parameter space. In brief, Latin Hypercube sampling partitions the input distributions into a predefined number of intervals (here 1000) with equal probability. Subsequently, a single sample per interval is extracted in an effort to evenly distribute sampling effort across all input values and hence reduce the number of samples needed to accurately represent the parameter space.

References

Andrade JL, Meinzer FC, Goldstein G, Schnitzer SA. 2005. Water uptake and transport in lianas and co-occurring trees of a seasonally dry tropical forest. *Trees* **19**: 282–289.

Clapp RB, Hornberger GM. 1978. Empirical equations for some soil hydraulic properties. *Water resources research* **14**: 601–604.

Cristiano PM, Campanello PI, Bucci SJ, Rodriguez SA, Lezcano OA, Scholz FG, Madanes N, Di Francescantonio D, Carrasco LO, Zhang Y-J. 2015. Evapotranspiration of subtropical forests and tree plantations: A comparative analysis at different temporal and spatial scales. *Agricultural and Forest Meteorology* **203**: 96–106.

Leuschner C, Coners H, Icke R. 2004. In situ measurement of water absorption by fine roots of three temperate trees: species differences and differential activity of superficial and deep roots. *Tree Physiology* **24**: 1359–1367.

Marshall JD, Cuntz M, Beyer M, Dubbert M, Kuehnhammer K. 2020. Borehole equilibration: testing a new method to monitor the isotopic composition of tree xylem water in situ. *Frontiers in Plant Science* **11**: 358.

McKay J. 1988. Sensitivity and uncertainty analysis using a statistical sample of input values. Uncertainty analysis.

McKay MD, Beckman RJ, Conover WJ. 1979. Comparison of three methods for selecting values of input variables in the analysis of output from a computer code. *Technometrics* **21**: 239–245.

Rüdinger M, Hallgren SW, Steudle E, Schulze E-D. 1994. Hydraulic and osmotic properties of spruce roots. *Journal of Experimental Botany* **45**: 1413–1425.

Sands R, Fiscus EL, Reid CPP. 1982. Hydraulic properties of pine and bean roots with varying degrees of suberization, vascular differentiation and mycorrhizal infection. *Functional Plant Biology* 9: 559–569.

Steudle E, Meshcheryakov AB. 1996. Hydraulic and osmotic properties of oak roots. *Journal of Experimental Botany* **47**: 387–401.

Figures and tables

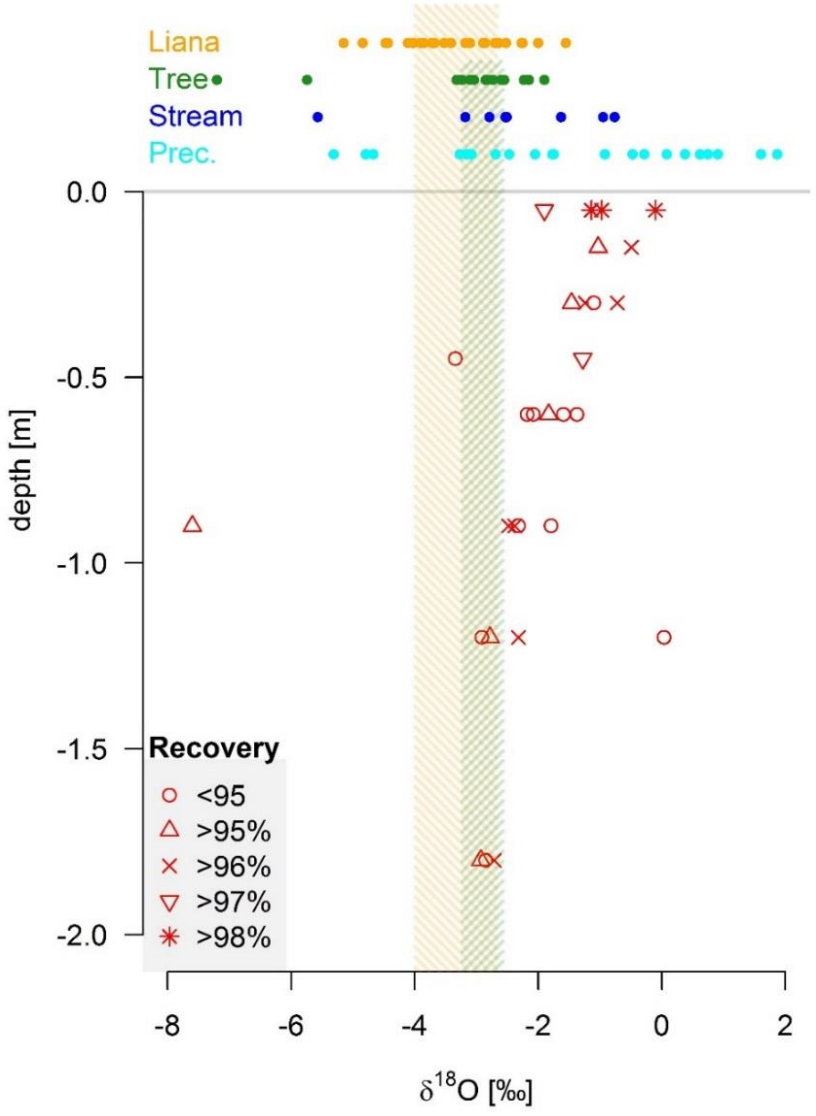

Fig. S1. Oxygen isotope composition ($\delta^{18}O$, in ‰ V-SMOW) of bulk soil water sampled at different depths (red), xylem water of lianas (orange) and trees (green), and from bulk stream (blue) and bulk precipitation water (cyan) in Laussat, French Guiana. Different soil $\delta^{18}O$ composition symbols indicate the extraction recovery rates, where 98% presents the generally pursued benchmark. Shaded areas show the Q25-Q75 intervals for lianas and trees in orange and green respectively.

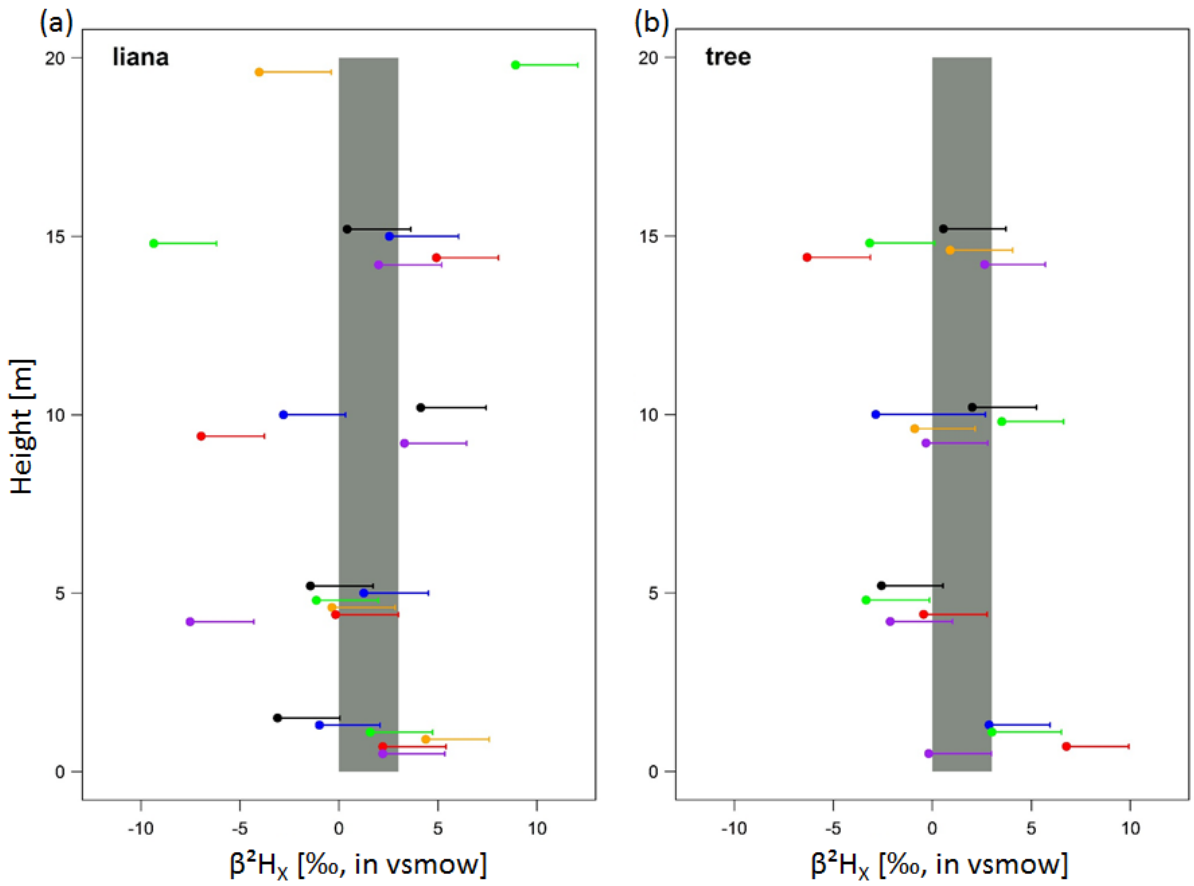

Fig. S2. Field measurements of normalized intra-individual δ^2H_X (β^2H_X) for six lianas (panel a) and six trees (panel b). Individuals are provided in different colors; liana species: ■ *Coccoloba sp.*, ■ sp.2, ■ sp.3, ■ *cf. rotundifolium Rich.*, ■ *Maripa cf violacea*, ■ *Maripa sp.*; tree species: ■ *Coussapoa sp.*, ■ *Vouacapoua americana*, ■ *Erisma nitidum*, ■ *Micropholis guyanensis*, ■ *Tapirira guyanensis*, ■ *Albizia pedicellaris*. Error whiskers are the combination of potential extraction and measurement errors of the isotope analyzer. The former presents a positive skew-normal distribution $SN_{empirical}(\xi = 0‰, \omega = 3‰, \alpha = +\infty)$. The full grey envelope delineates the acceptable variance from the stem mean (i.e. 3‰) according to the standard assumption of no variance along the length of a lignified plant, i.e the null model.

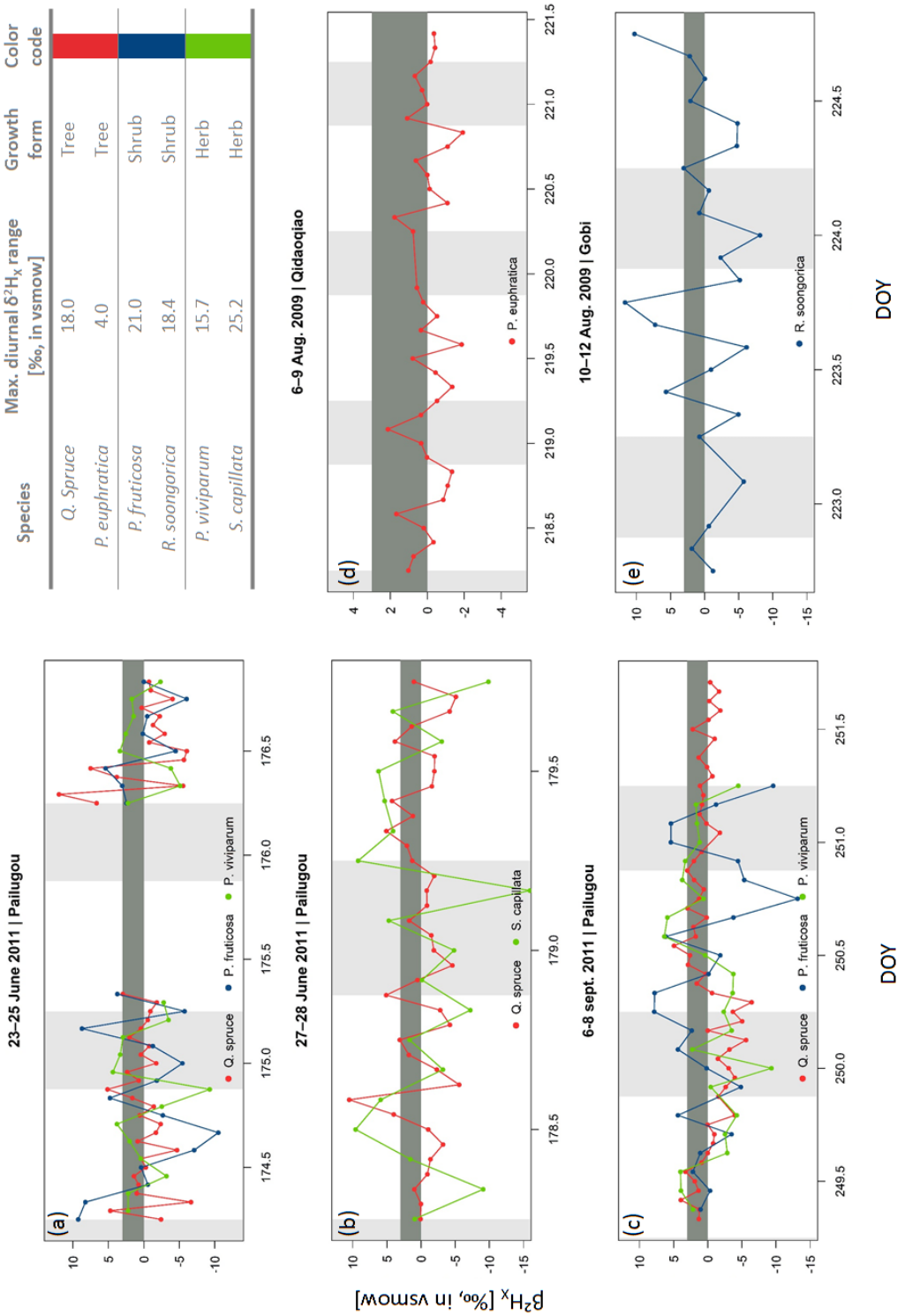

Fig. S3. High temporal field measurements of normalized δ^2H composition of xylem water (β^2H_X) of two trees (red, stem samples), two shrubs (blue, stem samples) and two herbs (green, root samples) species sampled in the Heihe River Basin (northwestern China) shown for the respective measurement periods. Timing and location of sampling are provided in the panel titles. Horizontal dark grey colored envelope delineates the acceptable variance from the stem mean (i.e. 3‰) according to the standard assumption of no variance along the length of a lignified plant. Light grey vertical envelopes mark the nighttime periods. The table provides the maximum measured diurnal δ^2H_X range per species.

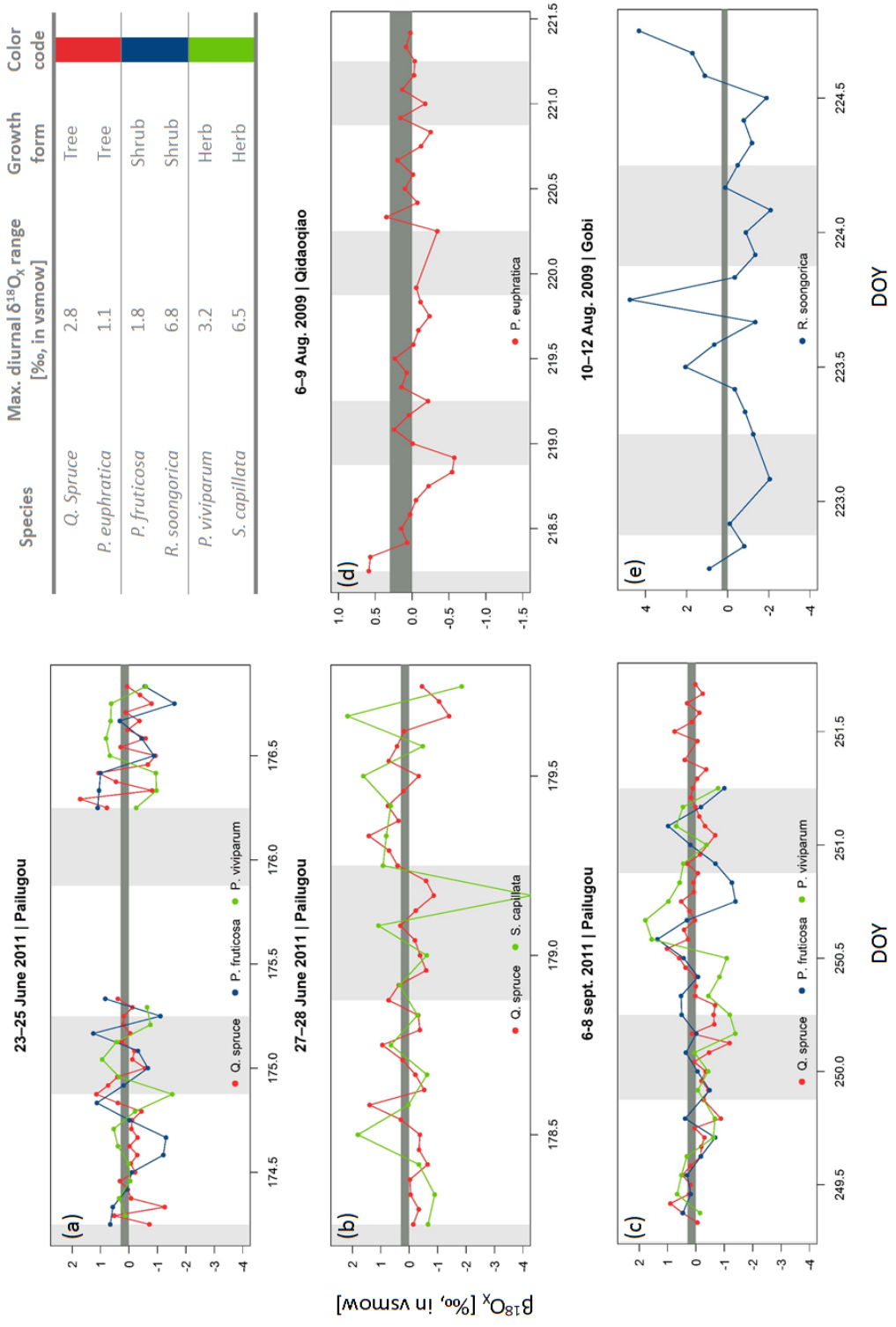

Fig. S4. High temporal field measurements of normalized $\delta^{18}O$ composition of xylem water ($\beta^{18}O_X$) of two trees (red, stem samples), two shrubs (blue, stem samples) and two herbs (green, root samples) in the Heihe River Basin (northwestern China) shown for the respective measurement period. Timing and location of sampling are provided in the panel title. Horizontal dark grey colored envelope delineates the acceptable variance from the stem mean (i.e. 0.3‰) according to the standard assumption of no variance along the length of a lignified plant. Light grey vertical envelopes mark the nighttime periods. The table provides the maximum measured diurnal $\delta^{18}O_X$ range per species.

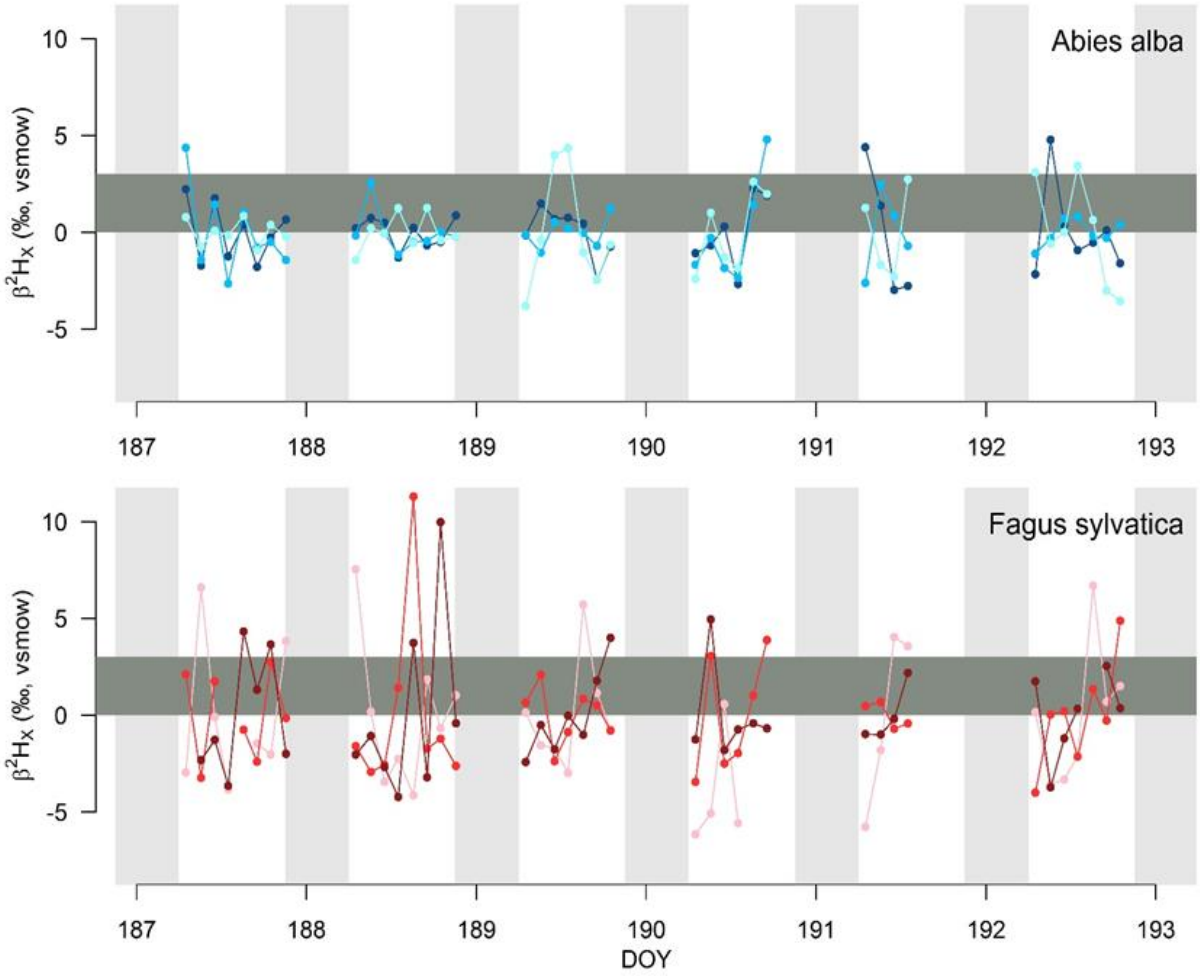

Fig. S5. High temporal field measurements of normalized δ^2H composition of xylem water (β^2H_X) of three *Abies alba* individuals (blue, branch samples) and three *Fagus sylvatica* individuals (red, branch samples) sampled during a drought period in July 2017 in the "Freiamt" field site in south-west Germany. Horizontal dark grey colored envelope delineates the acceptable variance from the stem mean (i.e. 3‰) according to the standard assumption of no variance along the length of a lignified plant. Light grey vertical envelopes mark the nighttime periods.

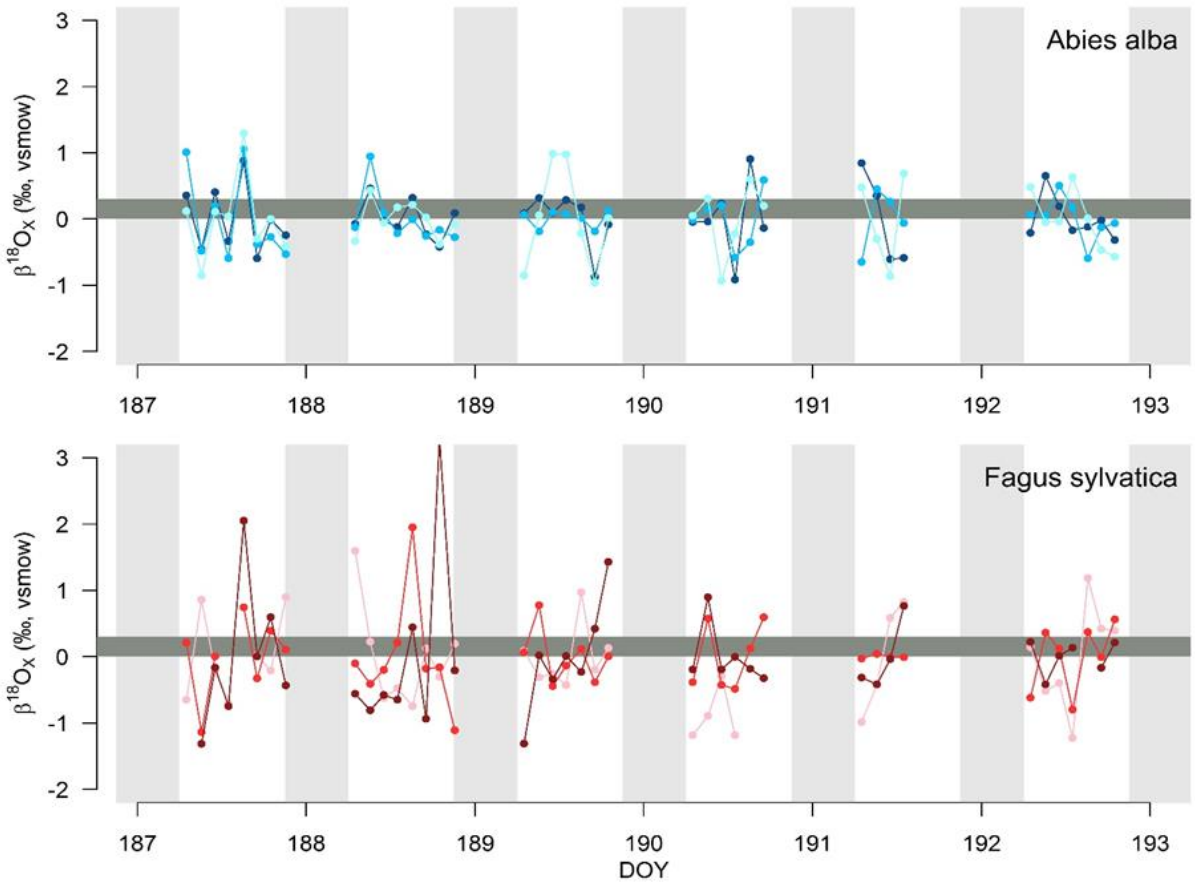

Fig. S6. High temporal field measurements of normalized $\delta^{18}O$ composition of xylem water ($\beta^{18}O_X$) of three *Abies alba* individuals (blue, branch samples) and three *Fagus sylvatica* individuals (red, branch samples) sampled during a drought period in July 2017 in the "Freiamt" field site in south-west Germany. Horizontal dark grey colored envelope delineates the acceptable variance from the stem mean (i.e. 0.3‰) according to the standard assumption of no variance along the length of a lignified plant. Light grey vertical envelopes mark the nighttime periods.

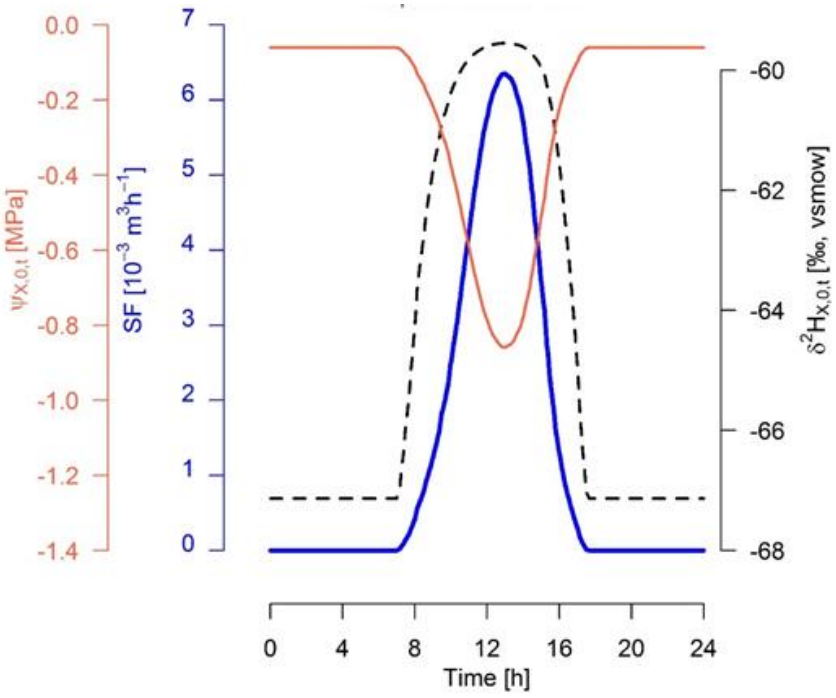

389

390

391 **Fig S7:** Sap flow rate (*SF*, blue line), δ^2H composition of xylem water at stem base ($\delta^2 H_{X,0,t}$
392 black dashed line) and water potential at stem base ($\Psi_{X,0,t}$, red line) shown for a single day.
393

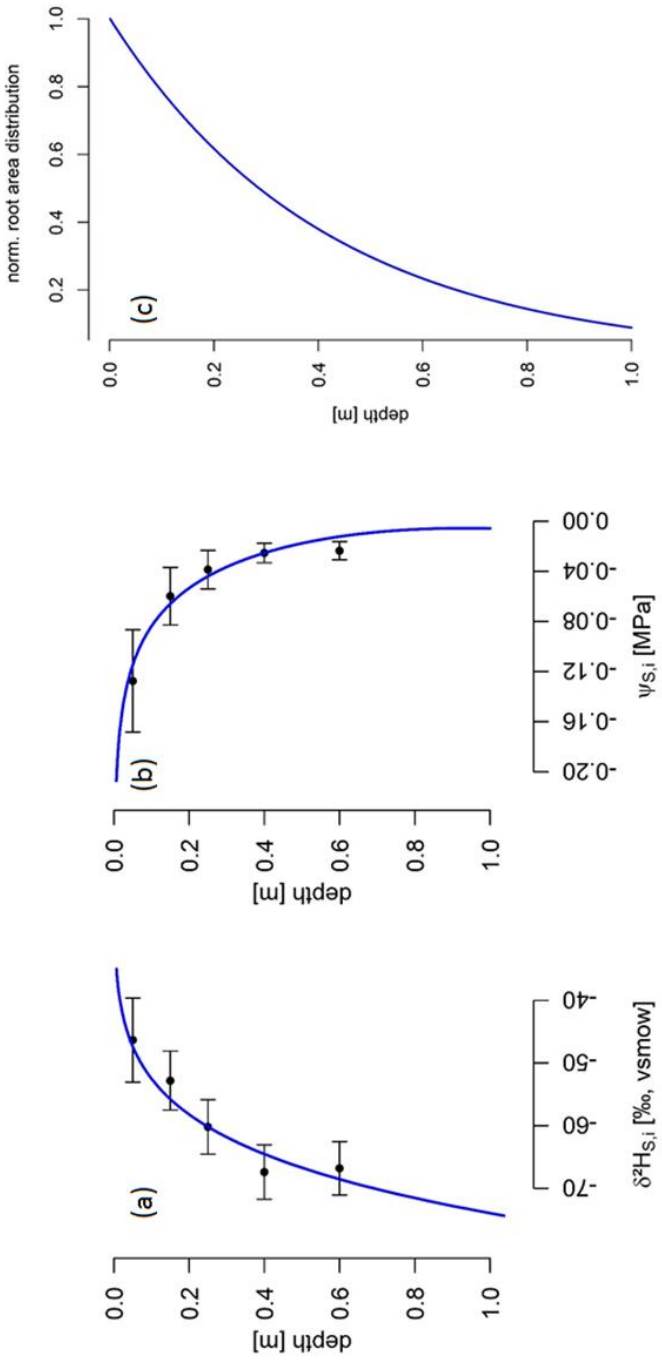

Fig. S8. (a) *²H* composition of soil water ($\delta^2H_{S,i}$) with depth, data from Meißner et al. (2012). **(b)** Soil water potential ($\Psi_{S,i}$) over the soil depth, data from Meißner et al. (2012). **(c)** The relative absorptive root area distribution with soil depths adapted from Jackson et al. (1995) and normalized to the topsoil. All equations and corresponding parameters for the fitted curves can be found in Table S1.

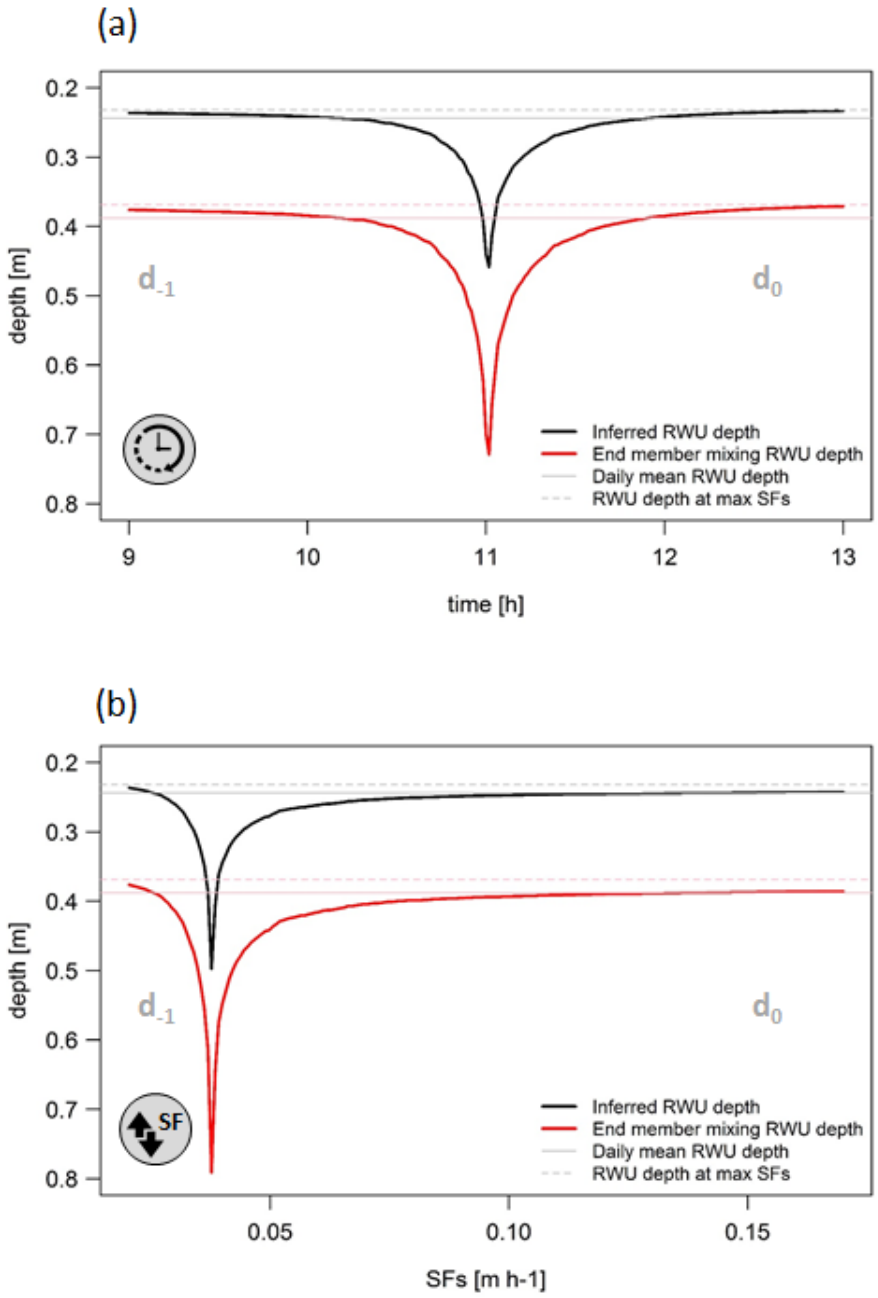

400

401 **Fig. S9.** Differences between the (RWU) depth derived from using either the direct inference
402 (black line) or the end member mixing (red line) approach. **Panel a:** The derived RWU depth
403 for a tree sampled at standard tree coring height (i.e. 1.30 m) having a sap flux density (SF_S) of
404 0.04 m h^{-1} (i.e. SF_V = 0.28 m h^{-1}), over the common sampling period (9:00 until 13:00). **Panel**
405 **b:** The derived RWU depth considering a tree sampled at standard tree coring height (1.30 m)
406 at 11:00, but which differs in SF_S. The grey and pink solid lines represent daily mean RWU
407 depth while the grey and pink dashed lines represent the RWU depth at peak sap flow activity,
408 respectively, for the direct inference and end-member mixing model approach. d_{-1} and d_0
409 indicate whether the derived RWU depth error corresponds to the previous or current day of
410 measurement.

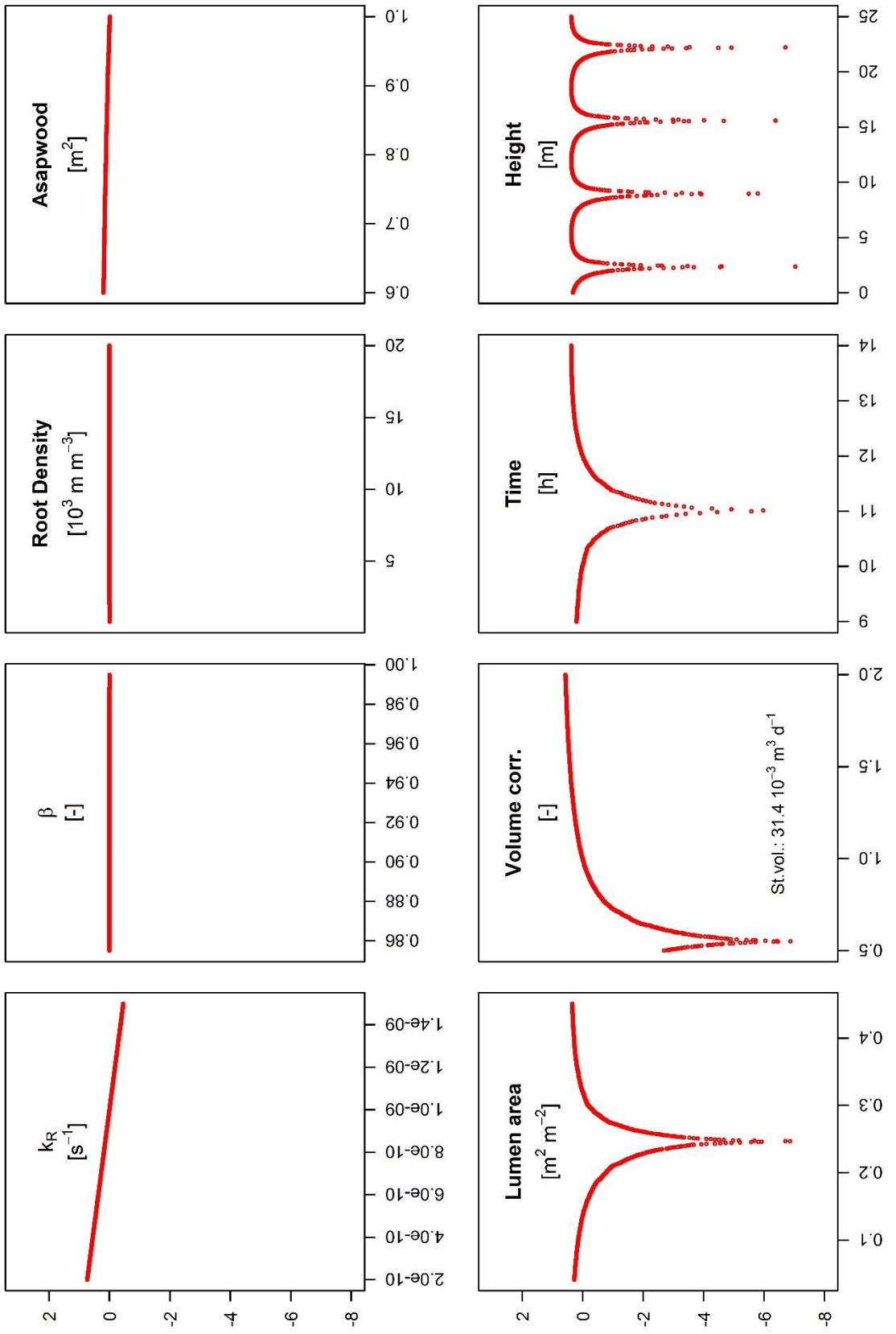
δ²Hₓ Bias [‰, in VSMOW]
k_R [s⁻¹]
β [-]
Root Density [10³ m m⁻³]
Asapwood [m²]
Lumen area [m² m⁻²]
Volume corr. [-]
St.vol.: 31.4 10⁻³ m³ d⁻¹
Time [h]
Height [m]

411

Fig. S10. Sensitivity analysis where all parameters are varied one-at-the-time as compared to the standard parameterization (see Table S1). For each studied variable, 1000 model runs were performed, studying the resulting δ^2H_X bias in comparison with the standard run. Each time, the studied parameter value was assigned randomly from a defined probability distribution or range using a Latin Hypercube scheme (see Table S2). The effective root radial conductivity (k_R, in s^{-1}), the β (-), and root density (in 10^3 m m^3) together form an informative proxy for the soil to root resistance. The lumen fraction (in m^2 m^{-2}), sapwood area (*Asapwood*, in m^2), and the total diurnal transported sap flow volume, i.e. net root water uptake (Volume corr., factor of standard run volume), provide an informative proxy for the sap flux density. (see Table S1). Time (in h) and height (in m) respectively represent the timing of sampling and the height of sample collection.

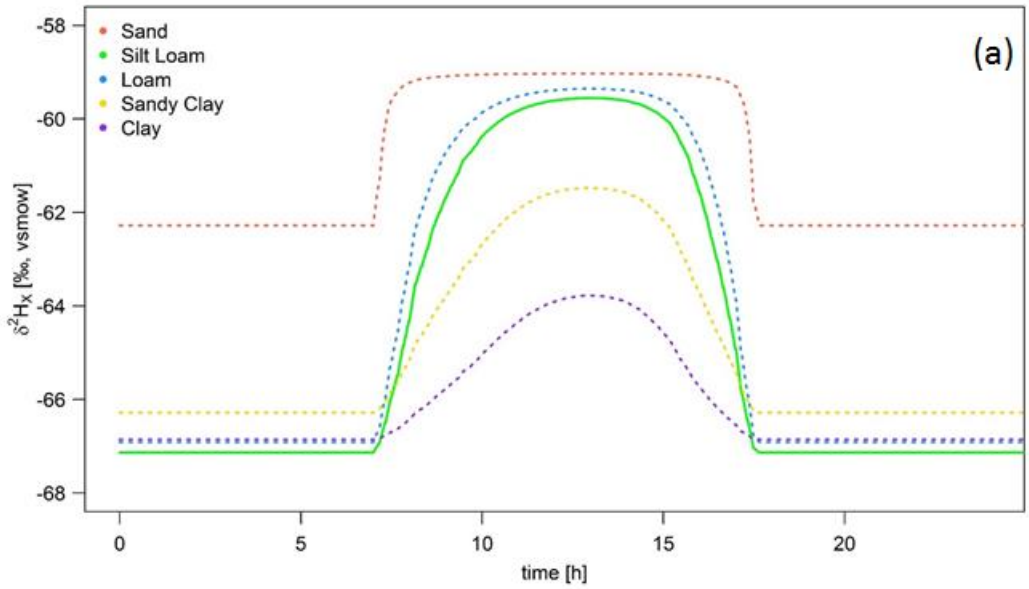
(a)
Sand
Silt Loam
Loam
Sandy Clay
Clay
-58
-60
-62
-64
-66
-68
δ²H_X [‰, vsmow]
0
5
10
15
20
time [h]

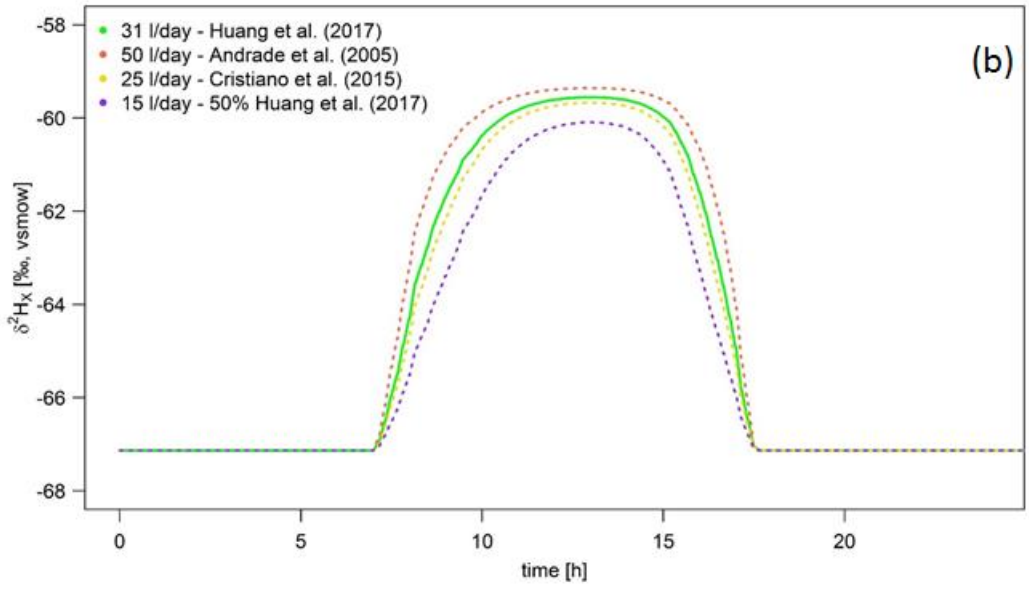
(b)
31 l/day - Huang et al. (2017)
50 l/day - Andrade et al. (2005)
25 l/day - Cristiano et al. (2015)
15 l/day - 50% Huang et al. (2017)
-58
-60
-62
-64
-66
-68
δ²H_X [‰, vsmow]
0
5
10
15
20
time [h]

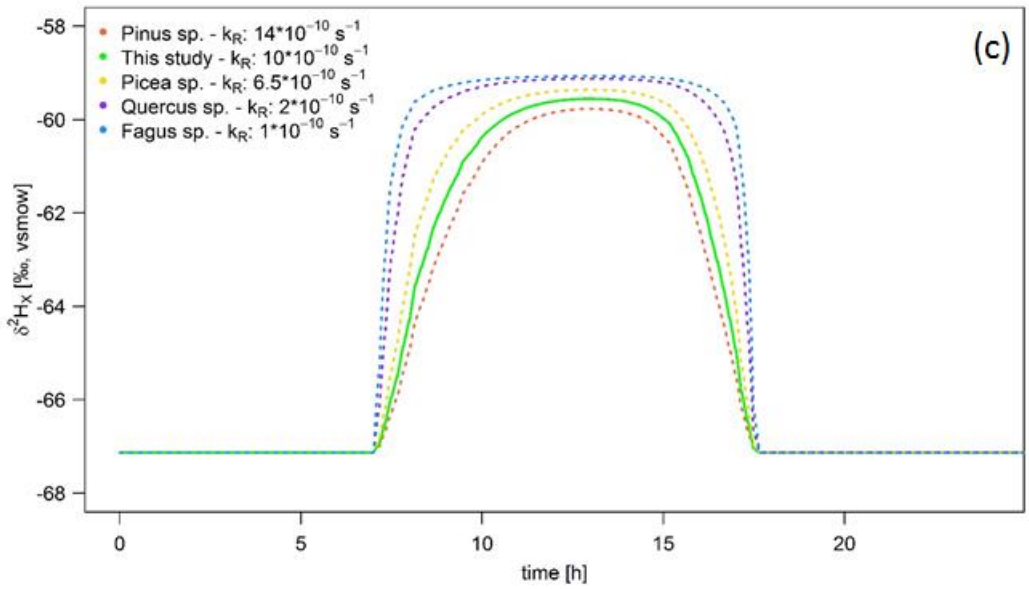
(c)
Pinus sp. - k_R: 14*10^-10 s^-1
This study - k_R: 10*10^-10 s^-1
Picea sp. - k_R: 6.5*10^-10 s^-1
Quercus sp. - k_R: 2*10^-10 s^-1
Fagus sp. - k_R: 1*10^-10 s^-1
-58
-60
-62
-64
-66
-68
δ²H_X [‰, vsmow]
0
5
10
15
20
time [h]

423

Fig. S11. Model sensitivity to (bio)physical parameters. The standard model run is shown by the solid green line in all panels. **Panel a:** fixed soil moisture and depth profile in the isotope composition of soil water ($\delta^2 H_{S,i}$), but with different soil types influencing the soil conductivity and soil water potential gradient in the soil ($\Psi_{S,i,t}$). Parameterization for each soil type is derived from Clapp & Hornberger (1978). **Panel b:** Impact of altering volumes of water taken up by the plant. **Panel c:** Effect of altering values of the effective root radial conductivity (k_R) values. Values are species-specific and are derived from the literature (Sands *et al.*, 1982; Rüdinger *et al.*, 1994; Steudle & Meshcheryakov, 1996; Leuschner *et al.*, 2004). In each panel all other parameters follow the standard plant parameterization (Table S1).

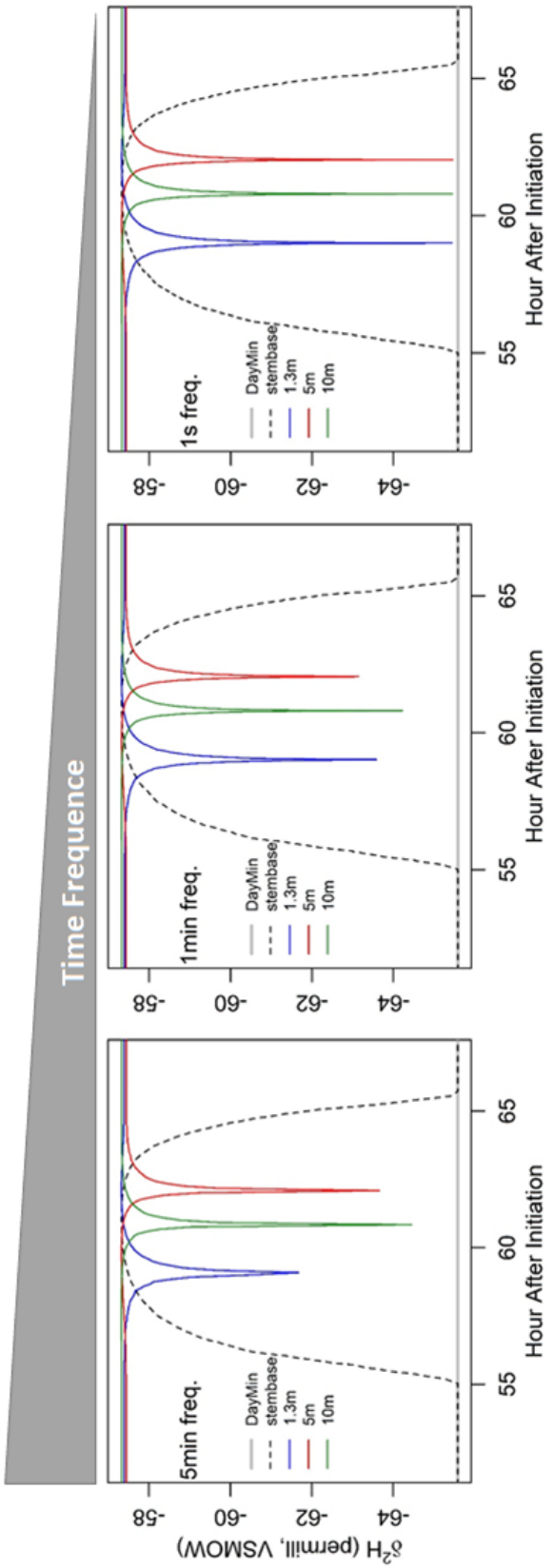

433

434 **Fig. S12.** Model simulations performed with varying temporal resolutions, i.e. 5min, 1min, and
435 1sec.

Table S1. An overview of the model standard parameterization of the present model, including sap flow, with corresponding references to literature.

Abbr.	Parameter	Unit	Value	Source
A_{Rtot}	The plants' total absorptive root area	m^2	$e^{0.88 \cdot \ln\left(\pi \cdot \left[\frac{DBH \cdot 10^2}{2}\right]^2\right) - 2}$	Čermák *et al.* (2006) $A_{Rtot} = 23.825\ m^2$
$A_{R,i}$	The absorptive root area distribution over soil layer *i*	m^2	$A_{Rtot} \cdot \beta^{100 \cdot z_i} \cdot (1 - \beta^{100 \cdot \Delta z})$	A_{Rtot} multiplied by the integrated root distribution of each soil layer adapted from Jackson *et al.* (1996)
			β =0.976	Huang *et al.* (2017)
$A_{SAPWOOD}$	Sapwood area	m^2	$\frac{1.582 \cdot [DBH \cdot 10^2]^{1.764}}{10^4}$	Meinzer *et al.* (2001)
Ax	Total lumen area	m^2	$LF \cdot A_{SAPWOOD}$	
B_i	The overall root length density per unit of soil, not necessarily limited to the studied plant.	$m\ m^{-3}$	$R_0 \cdot \beta^{100 \cdot z_i} \cdot \ln(\beta)$	Adapted from Huang *et al.* (2017) R_0= -438 688 β =0.976
DBH	Diameter at breast height	m	0.213	Huang *et al.* (2017)
$\delta^2 H_{S,i}$	^2H composition of soil water of the sampled soil layers	in ‰, VSMOW	$a + (z_i + b)^c$	Adapted from Meißner *et al.* (2012) …a: -73.98008 …b=0.001 …c=0.148735;
Δz	The thickness of each soil layer	m	0.001	
f_t	Temporal resolution	s^{-1}	1/60	
k_R	The effective root radial conductivity	s^{-1}	10^{-9}	Huang *et al.* (2017)

Table S1 (continuation)

Abbr.	Parameter	Unit	Value	Source
$K_{S,i}$	The soil hydraulic conductivity defined per soil depth	m s^{-1}	$K_{s,max} \cdot \left(\frac{\Psi_{sat}}{\Psi_{S,i,t}}\right)^{2+\frac{3}{b}}$	Huang *et al.* (2017)
			$K_{s,max}$= 7.2·10^{-6} m s^{-1}	Clapp & Hornberger (1978) [Table 2, silt loam soil]
			Ψ_{sat}= -0.786 m H_2O	Clapp & Hornberger (1978) [Table 2, silt loam soil]
			b = 5.30	Clapp & Hornberger (1978) [Table 2, silt loam soil]
LF	Lumen fraction per unit sapwood area	m^2 m^{-2}	0.136	Zanne *et al.* (2010) [Table 2]
SF_t	Instantaneous sap flow at time t	m^3 s^{-1}		Adapted from Huang *et al.* (2017) [derived from scenario 6, day 11]
$\Psi_{S,i,t}$	Water potential at a specific soil layer depth *i* and time *t*	m H_2O	$(a + b \cdot log(z_i) - c \cdot z_i^2) \cdot CT$	Adapted from Meißner *et al.* (2012) a: 19.8455·10^{-3} b: 44.8909·10^{-3} c: 25.5594·10^{-3} CT: 101.97 (i.e. conversion factor between MPa and m H_2O)

z_i the soil depth of the i^{th} soil layer (in m)

Table S2. An overview of the defined distribution and ranges used for the sensitivity analysis whose results are displayed in Fig S10.

Model Variable	Description	Unit	Distribution	Specification
Variables that provide an informative proxy for the soil to root resistance				
k_R	The effective root radial conductivity	s^{-1}	Uniform	St.=$10 \cdot 10^{-10}$, min = $2 \cdot 10^{-10}$, max = $15 \cdot 10^{-10}$
Root density	Integral of B_i for entire soil depth by changing R0 (see Table S1)	m	Uniform	St.= 4000, min = 1000, max = 20000
β	Factor defining root length density profile (see Table S1)	[-]	Uniform	St.= 0.976, min = 0.855, max = 0.995
Variables that provide an informative proxy for the sap flow velocity of a plant				
$A_{SAPWOOD}$	Sapwood area	m^2	Uniform	St.= 0.979, min = 0.6, max = 1
Lumen Fraction	Lumen fraction	$m^2\ m^{-2}$	Uniform	St.=0.136, min = 0.0411, max = 0.451
Volume corr.	Correcting factor of the daily total transported sap flow volume which in the standard run corresponds to 31.4 10^{-3} m^3	[-]	Uniform	St.= 1, min = 0.5, max = 2.0
Variables related to the sample collection protocol				
Height	Height of sampling	m	Uniform	St. = 1.3, min = 0, max = 25
Time	Timing of sampling	h	Uniform	St. = 12, min = 9; max = 14

With: *St.* parameter value of the standard run, *min* and *max* the minimum and maximum assigned value

References in figures and tables

Andrade JL, Meinzer FC, Goldstein G, Schnitzer SA. 2005. Water uptake and transport in lianas and co-occurring trees of a seasonally dry tropical forest. *Trees* **19**: 282–289.

Čermák J, Ulrich R, Staněk Z, Koller J, Aubrecht L. 2006. Electrical measurement of tree root absorbing surfaces by the earth impedance method: 2. Verification based on allometric relationships and root severing experiments. *Tree physiology* **26**: 1113–1121.

Clapp RB, Hornberger GM. 1978. Empirical equations for some soil hydraulic properties. *Water resources research* **14**: 601–604.

Huang C, Domec J, Ward EJ, Duman T, Manoli G, Parolari AJ, Katul GG. 2017. The effect of plant water storage on water fluxes within the coupled soil–plant system. *New Phytologist* **213**: 1093–1106.

Jackson RB, Canadell J, Ehleringer JR, Mooney HA, Sala OE, Schulze ED. 1996. A global analysis of root distributions for terrestrial biomes. *Oecologia* **108**: 389–411.

Leuschner C, Coners H, Icke R. 2004. In situ measurement of water absorption by fine roots of three temperate trees: species differences and differential activity of superficial and deep roots. *Tree Physiology* **24**: 1359–1367.

Meinzer FC, Goldstein G, Andrade JL. 2001. Regulation of water flux through tropical forest canopy trees: do universal rules apply? *Tree physiology* **21**: 19–26.

Meißner M, Köhler M, Schwendenmann L, Hölscher D. 2012. Partitioning of soil water among canopy trees during a soil desiccation period in a temperate mixed forest. *Biogeosciences* **9**: 3465–3474.

Rüdinger M, Hallgren SW, Steudle E, Schulze E-D. 1994. Hydraulic and osmotic properties of spruce roots. *Journal of Experimental Botany* **45**: 1413–1425.

Sands R, Fiscus EL, Reid CPP. 1982. Hydraulic properties of pine and bean roots with varying degrees of suberization, vascular differentiation and mycorrhizal infection. *Functional Plant Biology* **9**: 559–569.

Steudle E, Meshcheryakov AB. 1996. Hydraulic and osmotic properties of oak roots. *Journal of Experimental Botany* **47**: 387–401.

Zanne AE, Westoby M, Falster DS, Ackerly DD, Loarie SR, Arnold SEJ, Coomes DA. 2010. Angiosperm wood structure: global patterns in vessel anatomy and their relation to wood density and potential conductivity. *American Journal of Botany* **97**: 207–215.